RIS Selection Scheme for UAV-based Multi-RIS-aided Multiuser Downlink Network with Imperfect and Outdated CSI

Ankur Bansal, *Member, IEEE*, Neelima Agrawal, *Member, IEEE*, Keshav Singh, *Member, IEEE*, Chih-Peng Li, *Fellow, IEEE*, and Shahid Mumtaz, *Senior Member, IEEE*

***Abstract*—In this paper, we explore the use of reconfigurable intelligent surface (RIS) in unmanned aerial vehicle (UAV) based multiuser downlink communications, where a flying UAV serves multiple single antenna users through multiple RISs mounted on various buildings. More specifically, we consider the selection of RISs based on the outdated and imperfect channel state information (CSI) of the composite UAV-RIS-User channels at the UAV. After selection process, the UAV communicates to the user via the selected RISs and also with the direct link. Particularly, we derive an infinite series based expression for selection probability of RISs under both the outdated and imperfect CSI of composite channels based selection scheme. We also derive the statistical distribution of instantaneously received signal-to-noise ratio (SNR) under outdated and imperfect CSI conditions of both the direct and composite links at the user. Next, using the derived statistics, we analyze the network's performance in terms of the average coverage probability (ACP) and average bit error rate (ABER) over the complete UAV flight time. Moreover, we discuss the behavior of ACP and ABER for very small and very large values of UAV transmit power, respectively. It is depicted through numerical results that selecting more RISs from a group of small-sized RISs may not be as advantageous as selecting fewer RISs from a group of large-sized RISs. Moreover, we also demonstrate the effect of several system parameters such as number of RIS reflecting elements, number of selected RISs, the severity of UAV-RIS and RIS-User links, and the severity of imperfect and outdated CSI on the network's performance. The analytical results are corroborated with Monte-Carlo simulations.**

***Index Terms*—Reconfigurable intelligent surface (RIS), unmanned aerial vehicle (UAV), outage probability, nultiuser downlink communication, outdated channel state information (CSI), imperfect CSI, RIS selection schemes.**

I. Introduction

DUE to rapid growth in the mobile-ready devices and connections, fulfilling the high data-rate demand with the available limited spectrum resources is really challenging for upcoming communication systems. Along with this, the wireless communication systems are expected to cater to the low latency, ultra reliability and low energy consumption demands. To support such explosive growth of traffic demand and the massive connectivity of internet of things (IoT) devices, unmanned aerial vehicle (UAV), which acts as on-demand flying/aerial base stations (BSs), has recently emerged as a promising technology [1]–[4] and can be used to offload traffic, relay, broadcast, and collect information. Thus, UAV-assisted networks turn up as a key enabler to deal with higher data rate and massive connectivity demands in beyond 5G (B5G) and 6G wireless communication systems [5]–[10].

There are two types of UAVs, namely i) rotary-wing type and ii) fixed-wing type [5], [11], [12]. While multiple propellers are deployed at the UAV in case of a rotary-wing type UAV which hover over fixed position [11], a fixed-wing type UAV which generally moves in a curvilinear path at certain height [12], cannot have vertical movement. The fixed-wing type UAV takes less power in contrast to the rotary-wing type UAV, and therefore it is an important candidate for power-limited temporal wireless networks. However, in the urban areas, the communication signals between UAV and user equipment may be blocked due to high-rise building or other obstacles. Consequently, reconfigurable intelligent surface (RIS) has been proposed to address these challenges in UAV-based communications.

The RIS has the potential to improve the communication quality by adjusting the signal reflections in desired directions. In general, the RIS consists of an array of low cost and passive reflecting elements, each of which is able to reflect the incident signals by smartly adjusting the phase shift, which has the potential to improve the achievable data rate significantly [13], [14]. Due to these advantages over conventional amplify-and-forward and decode-and-forward relaying protocols, the RIS has been extensively investigated in recent literature [15]–[17]. Numerous research works in the areas of RIS-aided communications have been recently reported in [18]–[20]. An UAV-based RIS-assisted communication has been studied in [21], [22] and several schemes have been proposed to optimize the network performance. In [23], an efficient resource allocation algorithm has been investigated for RIS-assisted cognitive radio network (CRN). Motivated by the advantages of UAV and RIS, in this work we consider joint RIS-UAV system and explore UAV-based multiple RIS-assisted multiuser

This work was supported by the National Science and Technology Council of Taiwan, under Grants NSTC 111-2221-E-110-021 and NSTC 109-2221-E-110-050-MY3. (*Corresponding author: Keshav Singh.*)

Ankur Bansal is with the Department of Electrical Engineering, Indian Institute of Technology Jammu - 181 221, Jammu & Kashmir, India. (e-mail: ankur.bansal@iitjammu.ac.in).

Neelima Agrawal, Keshav Singh and Chih-Peng Li are with the Institute of Communications Engineering, National Sun Yat-sen University, Kaohsiung 80424, Taiwan, R.O.C. (e-mail: neelimaagrawal.01@gmail.com, {keshav.singh, cpli}@mail.nsysu.edu.tw).

Shahid Mumtaz is with the Department of Applied Informatics Silesian University of Technology Akademicka 16 44-100 Gliwice, Poland and the Department of Engineering, Nottingham Trent University, Nottingham NG1 4FQ, UK (e-mail: Dr.shahid.mumtaz@ieee.org).

communications.

The integration of UAV and RIS has recently come up as an important framework to enhance the energy efficiency and spectrum efficiency in B5G and 6G communications [24]–[30]. In [27], an algorithm has been proposed to jointly design active and passive beamforming and UAV's trajectory in RIS-assisted UAV networks. While the secrecy rate maximization problem has been formulated in [28] for jointly optimizing the transmit power, UAV trajectory, and RIS phase shifts, an iterative algorithm has been proposed in [30] to maximize the sum-rate of the RIS-assisted UAV orthogonal frequency-division multiple access (OFDMA) communication systems. Recently, considering practical models and designing a robust beamforming in RIS-assisted communications becomes very important. Accordingly, in [31], an algorithm for robust beamforming design has been proposed for RIS-aided communication where a multi-antenna access point serves a single-antenna user with the aid of an RIS. Similar to [31], the authors in [32] have jointly optimized hybrid access point energy beamforming, time allocation, receive beamforming, transmit power allocation at user, RIS energy and information reflection coefficients under the constraints of non-linear energy harvesting and imperfect channel state information (CSI) for RIS-aided wireless powered network. Furthermore, an algorithm for robust beamforming and resource allocation has been investigated in [33] for RIS-assisted hybrid massive multiple-input multiple-output (MIMO) uplink networks. However, the works [31]–[33] have investigated robust beamforming design algorithms for convention RIS-aided wireless communication systems and have not yet explored it in RIS-aided UAV-based networks. In [34]–[36], more practical RIS-aided UAV based communication systems have been studied. For example: the authors in [34] have studied an RIS-aided millimeter-Wave UAV communication and focused on learning-based design of robust beamforming at the UAV, phase shifts at the RIS along with the UAV trajectory in order to enhance the sum secrecy rate. In parallel to [35], a robust resource allocation and the UAV's trajectory design algorithm has been proposed for RIS-aided secure UAV communications. A deep reinforcement learning (DRL) algorithm has been investigated in [36] to optimize power control, phase shifts at the RIS, and the UAV trajectory for RIS-assisted ground-aerial non-orthogonal multiple access (NOMA) communication system. However, the existing works in [24]–[36] have considered a single RIS-assisted network with or without UAV and focused only on optimization and did not analyze the network's performance in terms of the outage probability. Consequently, investigating RIS selection schemes and analyzing their outage performance metric in UAV-based multiple RIS-aided multiuser communication network become an interesting and important problem. To the best of our understanding, the RIS selection by the UAV based on the outdated and imperfect channel state information (CSI) of the composite UAV-RIS-User channels has not been explored analytically in the literature of RIS-assisted UAV-based multiuser downlink communications. Motivated by the above fact, we emphasize on analytical performance of an UAV-based multiple RIS-assisted multiuser downlink network considering the availability of direct UAV-user links. The paramount contributions of this work are as follows:

- An UAV-based multiple RIS-assisted multiuser downlink communication network is considered, where a rotary-wing type moving UAV communicates to several downlink users in orthogonal spectrum bands through a direct link and few *selected* RISs. The RIS selection is done at the UAV based on the outdated and imperfect CSIs of the composite UAV-RIS-User channels.
- For outdated and imperfect CSI based RIS selection scheme, we derive an expression for the probability of selecting a set of RISs (amongst the total RISs available) in the form of a single integral. Although, the series-based expression for the selection probability is obtained for the case when only one RIS (with the worst channel gain of composite channel) does not get selected. Moreover, the approximate statistical distribution of the instantaneous signal-to-noise ratio (SNR) under the imperfect and outdated CSIs of both the direct as well as composite fading links at a given user is derived by following the Rician fading distribution for all the communication links.
- By using the cumulative distribution function (CDF) of instantaneous SNR at user, we derive the series-based expressions for average coverage probability (ACP) and average bit error rate (ABER) over the entire flight duration of the UAV. In addition, we analytically evaluate the ACP performance under low transmit power regime to observe the rate of rise in ACP values. Similarly, we also derive the asymptotic ABER expressions under high transmit power conditions and observe that it varies with number of selected RISs only.
- Through numerical results, it is depicted that the network with small number of selected RISs from a set of large-sized RISs provides better network performance as compared to the one with large number of selected RISs from a pool of small-sized RISs. Furthermore, it is depicted through numerical results that increasing the reflecting elements beyond a certain limit does not yield significant improvement to the network performance, under a given system settings.
- At last, we demonstrate the effect of various system parameters and channels condition such as number of RISs selected and available in the network, and severity of imperfect and outdated CSI conditions, and severity conditions of UAV-RIS and RIS-User channel fading, etc., on the network's performances.

Framework of the paper: The remaining parts of the paper is structured as follows. Section II represents the considered system framework along with channel model for the considered UAV-based multiple RIS-aided multiuser downlink network. While Section III depicts the approximate statistical analysis of SNR at user, Section IV describes the schemes for selection of RISs by the UAV based on the outdated and imperfect CSI knowledge. The ACP and ABER under the imperfect and outdated CSI conditions at user are analyzed in Section V for the entire flight duration of the UAV. Section VI represents the detailed simulation results and Section VII concludes the findings of the paper.

Symbols and notations: Throughout the paper, we utilize the following symbols and notations. A matrix and a vector are denoted by The uppercase and lowercase boldface letters (for-instance: $\mathbf{A}$ and $\mathbf{a}$), respectively. While the hermitian of vector $\mathbf{a}$ is represented as $\mathbf{a}^{\mathrm{H}}$, $\mathbf{I}_M$ and $\mathbf{1}_{M\times 1}$ signify an identity matrix of size $M \times M$ and a column vector of all ones, respectively. The symbols $||\cdot||^2$ and the $||\mathbf{a}||$ represent the square norm of a vector and the distance of vector $\mathbf{a}$ from origin, respectively. $\mathcal{CN}(\cdot,\cdot)$ and $\mathbb{C}$ indicate the complex Gaussian distribution and a set of complex numbers, respectively. Moreover, the expectation operator is denoted by $\mathbb{E}[\cdot]$.

II. System Model

Fig. 1 shows the system model for UAV-assisted RIS-aided multiuser communication network, where a flying UAV having single transmit antenna serves K single-antenna based users in orthogonal spectrum bands via direct as well as multiple reflected links through RISs.

A. Preliminaries

The complete UAV flight time (denoted by T_C) is divided into T equal time slots with length $\delta_t = \frac{T_C}{T}$, for $t \in \mathbb{T}$, $\mathbb{T} = 1, 2, \ldots, T$ [34], [35], [37]. Normally, we choose T to be large enough so that the UAV location during each time slot can be considered as fixed. It is considered that the UAV flies over a horizontal $X-Y$ plane at a constant height H_U. The initial and final location coordinates of the UAV in a 3-D system are taken as $\boldsymbol{\chi}_U[t] = (x_U[0], y_U[0], H_U)$ and $\boldsymbol{\chi}_U[T] = (x_U[T], y_U[T], H_U)$, respectively, whereas in an arbitrary time slot t, the location coordinate may be considered as $\boldsymbol{\chi}_U[t] = (x_U[t], y_U[t], H_U)$ such that UAV speed over $X-Y$ plane is $v[t] = \frac{||\boldsymbol{\chi}_U[t] - \boldsymbol{\chi}_U[t-1]||}{\delta_t}$, in the given time slot t. In order to serve K ground users, frequency division multiple access (FDMA) scheme is used at the UAV in each time slot where same amount of bandwidth is allocated to all the users orthogonally. We also assume that the considered network has M RISs, each having N reflecting elements, for serving a user in an orthogonal spectrum. The location coordinate of m-th RIS and k-th ground user are taken as $\boldsymbol{\chi}_{R_m} = (x_{R_m}, y_{R_m}, z_{R_m})$ and $\boldsymbol{\chi}_k = (x_k, y_k, 0)$, respectively, where $m \in \mathbb{M}$, $\mathbb{M} = \{1, 2, \ldots, M\}$ and $k \in \mathbb{K}$, $\mathbb{K} = \{1, 2, \ldots, K\}$.

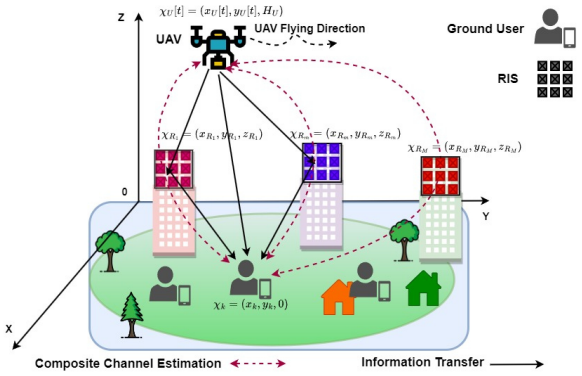

Fig. 1: UAV-based multiple RIS-aided multiuser communication network.

B. Channel Model

We assume that all the downlink channels considered in this work undergo multipath fading along with the existence of a non-zero LoS component. Hence, all the channel coefficients are modelled with a complex Gaussian distribution with non-zero mean such that the envelope of the complex channel coefficient follows Rician distribution. The channel coefficient of the k-th direct link between the UAV and the User in time slot t is considered as $h_{0,k}[t] \sim \mathcal{CN}\left(\mu_{0,k}[t], \frac{\alpha^2 \Omega_{0,k}}{d^{\beta}_{0,k}[t]}\right)$; where $d_{0,k}[t] = ||\boldsymbol{\chi}_U[t] - \boldsymbol{\chi}_k||$ is the distance between the UAV and k-th user over given time slot; for k-th direct channel, $\mu_{0,k}[t]$ is the mean in t-th time slot and $\Omega_{0,k}$ is normalized average gain; $\alpha = \frac{\lambda}{4\pi}$ is a constant denoting the losses at wavelength λ; and β represents path loss exponent. If $\mathbf{h}_m[t]$ denotes the m-th UAV-RIS channel vector, $m \in \mathbb{M}$, over time slot t, we may define $\mathbf{h}_m[t] \sim \mathcal{CN}\left(\mu_m[t]\mathbf{1}_{N\times 1}, \frac{1}{g_m[t]}\mathbf{I}_N\right)$. It may be noted that for two different values of $m \in \mathbb{M}$, vectors $\mathbf{h}_m[t]$ are independent but non-identically distributed due to different distances of the corresponding RISs from the UAV. However, all the elements of a vector $\mathbf{h}_m[t]$, i.e., $h_{m,n}[t]$, $n = 1, 2, \ldots, N$, are independent and identically distributed (i.i.d.) as complex Gaussian random variable (RV) with mean $\mu_m[t]$ and variance $g_m^{-1}[t]$; where $g_m[t] = \frac{d^{\beta}_m[t]}{\alpha^2 \Omega_m}$ with Ω_m being the normalized average gain of the m-th UAV-RIS link and $d_m[t] = ||\boldsymbol{\chi}_U[t] - \boldsymbol{\chi}_{R_m}||$ is the Euclidean distance of the m-th RIS from the UAV in the t-th time slot[1]. Further, we assume that $\mathbf{f}_{m,k}$ denotes the $\{m,k\}$-th RIS-User channel vector defined as $\mathbf{f}_{m,k} \sim \mathcal{CN}\left(\nu_{m,k}\mathbf{1}_{N\times 1}, \frac{\alpha^2 \Lambda_{m,k}}{d^{\beta}_{m,k}}\mathbf{I}_N\right)$, where $d_{m,k} = ||\boldsymbol{\chi}_{R_m} - \boldsymbol{\chi}_k||$ is the distance of the k-th user from the m-th RIS, $\nu_{m,k}$ denotes mean, and $\Lambda_{m,k}$ represents normalized average gain of the considered RIS-User link.

C. Transmission Scheme

To establish a communication link with a ground user, at first, a set of RISs is selected by the UAV based on the available instantaneous CSI (which is practically imperfect and outdated) of the composite UAV-RIS-User links. Secondly, the information signal is transmitted by the UAV over the direct path as well as cascaded paths via selected RISs only. Note that perfect channel estimation is an important problem in RIS-aided communications, especially under the consideration of dynamic UAV. Recently, many works have been reported on the CSI estimation in RIS-aided communication systems [38]–[40], however, practically, the moving UAV can only manage to have imperfect and outdated CSI of composite UAV-RIS-User channels. If the selected J RISs (in a given time slot t) have indices $m_1, m_2, \ldots, m_J \in \mathbb{M}$, we can write the received signal at k-th user as

$$y_k[t] = \sqrt{\tilde{P}_{U,k}[t]}\left(h_{0,k}[t] + \sum_{j=1}^{J} \mathbf{f}^{\mathrm{H}}_{m_j,k}\boldsymbol{\Theta}_{m_j}[t]\mathbf{h}_{m_j}[t]\right)x_k[t] + e_k[t], \quad (1)$$

[1]It may be noted that the location coordinate of an RIS refers to the location coordinate of the center of the reflecting surface.

where matrix $\mathbf{\Theta}_{m_j}[t]$ is a diagonal matrix of size $N \times N$, generally known as reflection matrix of an RIS, with n-th element representing the reflection coefficient in time slot t as $\theta_{m_j,n}[t] = \rho_{m_j,n}[t]e^{j\phi_{m_j,n}[t]}$. It may be noted that each reflection coefficient has a controllable amplitude ($\rho_{m_j,n}[t]$) and a controllabe phase ($\phi_{m_j,n}[t]$), for all $m_j \in \mathbb{M}$, $n \in \mathbb{N}$. Over a time slot t, the additive white Gaussian noise (AWGN) at k-th user is denoted as $e_k[t] \sim \mathcal{CN}(0, \sigma_k^2)$ and the power utilized at UAV is $\tilde{P}_{U,k}[t]$ for the downlink transmission of k-th user's data symbol $x_k[t]$. It is assumed that symbol $x_k[t]$ has unit norm, for all $k \in \mathbb{K}, t \in \mathbb{T}$.

Let the UAV posses an overall power of P_U for it's complete flight operation including hovering, flying, and data transmission, the amount of power accessible at UAV for the communication purpose would be $\tilde{P}_U = P_U - P_p$, where P_p denotes the propulsion power of the UAV needed for hovering. Following [41], we can calculate P_p as

$$P_p = \left[P_0 + \frac{3P_0 v^2[t]}{u_{tip}^2} + \frac{1}{2}d_f \rho_a s A v^3[t]\right] + P_1\left[\sqrt{1 + \frac{v^4[t]}{4v_0^4}} - \frac{v^2[t]}{2v_0^2}\right]^{1/2}, \quad (2)$$

where constants P_0, P_1 denotes the blade profile power and induced power of the UAV; u_{tip} is speed of rotor blade; v_0 denotes mean velocity while hovering; ρ_a and A are air density and rotor disc area, respectively; s is the solidity of rotor and d_f is the fuselage drag. Moreover, the total accessible power $\tilde{P}_U$ should be utilized over all the users and time slots and thus, must satisfy the constraint as $\tilde{P}_U = \sum_{t=1}^{T}\sum_{k=1}^{K}\tilde{P}_{U,k}[t]$.

III. Statistical Distribution of SNR with Imperfect and Outdated CSI

In this section, we derive the approximate analytical expression for the statistical distribution of instantaneous SNR received at k-th user during t-th time slot under the assumption of imperfect and outdated CSI at the user. Let us first write the instantaneous SNR at k-th user node under the perfect CSI case, by following (1), as

$$\begin{aligned}\Gamma_k[t] &= \frac{\tilde{P}_{U,k}[t]}{\sigma_k^2}\left|h_{0,k}[t] + \sum_{j=1}^{J}\mathbf{f}_{m_j,k}^{\mathrm{H}}\mathbf{\Theta}_{\boldsymbol{m_j}}[\boldsymbol{t}]\mathbf{h}_{m_j}[t]\right|^2, \\ &\approx \frac{J\tilde{P}_{U,k}[t]}{\sigma_k^2}\left[|h_{0,k}[t]|^2 + \sum_{j=1}^{J}\left|\mathbf{f}_{m_j,k}^{\mathrm{H}}\mathbf{\Theta}_{m_j}[t]\mathbf{h}_{m_j}[t]\right|^2\right], \\ &\triangleq \frac{J\tilde{P}_{U,k}[t]}{\sigma_k^2}\left[|h_{0,k}[t]|^2 + \sum_{j=1}^{J}\left|X_{m_j,k}[t]\right|^2\right], \end{aligned} \quad (3)$$

where we use the approximation $|A_0 + A_1 + \ldots + A_J|^2 \approx J(|A_0|^2 + |A_1|^2 + \ldots + |A_J|^2)$, for tractability of analysis. For practical reflection coefficients defined in Subsection II-C, we have

$$\begin{aligned}&X_{m_j,k}[t] \\ &= \sum_{n=1}^{N}\rho_{m_j,n}[t]|f_{m_j,k,n}||h_{m_j,n}[t]|e^{j(\phi_{m_j,n}[t] - \psi_{m_j,k,n} - \varphi_{m_j,n}[t])},\end{aligned} \quad (4)$$

where $\psi_{m_j,k,n}$ and $\varphi_{m_j,n}[t]$ denote the phase angles of n-th channel coefficients $f_{m_j,k,n}$ and $h_{m_j,n}[t]$, respectively, of RIS$_{m_j}$-User$_k$ and UAV-RIS$_{m_j}$ channels. It may be noted that the value of reflection phase at n-th RIS element (i.e., $\phi_{m_j,n}[t]$) can be chosen through optimization-based resource allocation[2] for FDMA-based multi-user communication by maximizing the key performance metrics (such as the sum rate over all K Users) [42]. Furthermore, it is reasonable to assume that for optimized phase shift values at RIS, the phase difference in (4) is sufficiently small and can be neglected for the purpose of performance analysis. Hence, for perfect CSI case with ideal reflections at RISs, for all $m_j \in \mathbb{M}$ and $t \in \mathbb{T}$, we can rewrite (4) as

$$X_{m_j,k}[t] = \sum_{n=1}^{N}|f_{m_j,k,n}||h_{m_j,n}[t]| \triangleq \sum_{n=1}^{N}X_{m_j,k,n}[t]. \quad (5)$$

Since $\mathbf{f}_{m_j,k}$ and $\mathbf{h}_{m_j}[t]$ are independent complex Gaussian random vectors with non-zero means, the mean and the variance of product of the absolute of their n-th elements can be obtained by following [43] as

$$\begin{aligned}&\mathbb{E}[X_{m_j,k,n}[t]] \\ &\quad = \frac{\pi}{4}\frac{u_{m_j}v_{m_j,k}}{\sqrt{\mathcal{K}_{1,m_j}[t]\mathcal{K}_{2,m_j}}}\mathcal{L}_{\frac{1}{2}}\Big(-\mathcal{K}_{1,m_j}[t]\Big)\mathcal{L}_{\frac{1}{2}}\Big(-\mathcal{K}_{2,m_j}\Big), \\ &\mathbb{V}[X_{m_j,k,n}[t]] \\ &\quad = u_{m_j}^2 v_{m_j,k}^2\left(1 + \frac{1}{\mathcal{K}_{1,m_j}[t]}\right)\left(1 + \frac{1}{\mathcal{K}_{2,m_j}}\right) \\ &\qquad - \mathbb{E}^2[X_{m_j,k,n}[t]],\end{aligned} \quad (6)$$

respectively, where $\mathcal{K}_{1,m_j}[t] = u_{m_j}^2 g_{m_j}[t]$ with $u_{m_j} = |\mu_{m_j}|$ and $\mathcal{K}_{2,m_j} = \frac{v_{m_j,k}^2 d_{m_j,k}^{\beta}}{\alpha^2 \Lambda_{m_j,k}}$ with $v_{m_j,k} = |\nu_{m_j,k}|$; $\mathcal{L}_{\frac{1}{2}}(\cdot)$ defines the Laguerre polynomial [44]; and $\mathbb{V}[\cdot]$ denotes the variance operator. For sufficiently large values of N, we can consider that $X_{m_j,k}[t]$ (defined in (5)) follows real Gaussian distribution (as per the central limit theorem) with mean $\mathbb{E}[X_{m_j,k}[t]] = N\mathbb{E}[X_{m_j,k,n}[t]]$ and variance $\mathbb{V}[X_{m_j,k}[t]] = N\mathbb{V}[X_{m_j,k,n}[t]]$.

A. Characterization of SNR under Imperfect and Outdated CSI at User

Due to the mobility of the UAV and the time varying nature of the channel, the CSI available at the ground user in a given time slot may be delayed and hence becomes outdated. Furthermore, there may be errors while estimating the direct as well as the composite channel coefficients at the user nodes.

[2]This approach is widely adopted in the literature for RIS-assisted communication networks [23]-[25], however, the formulation and solving of such optimization problems using standard optimization methods is a cumbersome and tedious mathematical problem that requires a separate independent study.

Considering both the outdated and imperfect CSI at the ground users, we can redefine the expression for the approximate instantaneous SNR from (3) as

$$\check{\Gamma}_k[t] \approx \frac{J\tilde{P}_{U,k}[t]}{\sigma_k^2}\left[\left|\check{h}_{0,k}[t]\right|^2 + \sum_{j=1}^{J}\left|\check{X}_{m_j,k}[t]\right|^2\right], \quad (7)$$

where $\check{h}_{0,k}[t]$ and $\check{X}_{m_j,k}[t]$ represent the imperfect and outdated versions of $h_{0,k}[t]$ and $X_{m_j,k}[t]$, respectively. For the k-th direct UAV-User channel, $\check{h}_{0,k}[t]$ can be defined as [34]

$$\check{h}_{0,k}[t] = \varrho_k[t]h_{0,k}[t] + \varrho_k[t]h_{e,k}[t] + \sqrt{1-\varrho_k^2[t]}h_{d,k}[t], \quad (8)$$

where $h_{e,k}[t] \sim \mathcal{CN}(0, 2\sigma_{e,k}^2)$ denotes the complex estimation error and $h_{d,k}[t] \sim \mathcal{CN}(0, 2\sigma_{d,k}^2)$ represents the error due to the delay at k-th user node, and $\varrho_k[t]$ is the correlation coefficient between the estimated and outdated CSIs at the k-th user node in t-th time slot. For Clarke's fading model with a delay of $\tau_{d,k}[t]$ between the estimated and the outdated CSI at k-th user node in t-th time slot, the correlation coefficient can be given as $\varrho_k[t] = \mathcal{J}_0(2\pi f_{d,k}[t]\tau_{d,k}[t])$, where $\mathcal{J}_0(\cdot)$ is the zeroth order Bessel function of first kind, and $f_{d,k}[t]$ is the Doppler spread at k-th user node in time slot δ_t due to the movement of the UAV.

Similarly, for the composite UAV-RIS-User channel with m_j-th RIS and k-th user, $\check{X}_{m_j,k}[t]$ can be defined as [34]

$$\begin{aligned}\check{X}_{m_j,k}[t] =& \varrho_{m_j,k}[t]X_{m_j,k}[t] + \varrho_{m_j,k}[t]X_{e,k}[t] \\ &+ \sqrt{1-\varrho_{m_j,k}^2[t]}X_{d,k}[t], \quad (9)\end{aligned}$$

where $X_{e,k}[t] \sim \mathcal{N}(0, \sigma_{e,k}^2)$ denotes the real estimation error and $X_{d,k}[t] \sim \mathcal{N}(0, \sigma_{d,k}^2)$ represents the real-valued error due to the delay at k-th user node, and $\varrho_{m_j,k}$ is the correlation coefficient between the estimated and outdated CSIs of the composite channel at the k-th user node in t-th time slot, defined as $\varrho_{m_j,k} = \mathcal{J}_0(2\pi f_{d,m_j,k}[t]\tau_{d,m_j,k}[t])$, with $\tau_{d,m_j,k}[t]$ and $f_{d,m_j,k}[t]$ being the the delay and the Doppler spread of the composite channel at k-th user node in t-th time slot (through m_j-th RIS) due to the movement of the UAV.

B. Approximate Distributions of Channel Gains under Imperfect and Outdated CSI at User

Since $h_{0,k}[t] \sim \mathcal{CN}\left(\mu_{0,k}[t], g_{0,k}^{-1}[t]\right)$, where $g_{0,k}^{-1}[t] \triangleq \frac{\alpha^2\Omega_{0,k}}{d_{0,k}^{\beta}[t]}$, following (8) we can get $\check{h}_{0,k}[t] \sim \mathcal{CN}\left(\varrho_k[t]\mu_{0,k}[t], \check{g}_{0,k}^{-1}[t]\right)$, where

$$\begin{aligned}\check{g}_{0,k}^{-1}[t] &= \varrho_k^2[t]g_{0,k}^{-1}[t] + 2\varrho_k^2[t]\sigma_{e,k}^2 + 2(1-\varrho_k^2[t])\sigma_{d,k}^2, \\ &\triangleq g_{0,k}^{-1}[t]\left[\varrho_k^2[t](1+\delta_{0,e,k}^2) + (1-\varrho_k^2[t])\delta_{0,d,k}^2\right], \quad (10)\end{aligned}$$

where $\delta_{0,a,k}^2[t] = 2\sigma_{a,k}^2 g_{0,k}[t]$, $a \in \{e, d\}$, is the normalized error variance for the direct link. With this, the $\check{g}_{0,k}[t]|\check{h}_{0,k}[t]|^2$ will follow non-central chi-square (NCCS) distribution with two degrees of freedom (DoF) and non-centrality parameter $\mathcal{K}_{0,k}[t] = \varrho_k^2[t]|\mu_{0,k}[t]|^2\check{g}_{0,k}[t]$. Thus, the CDF and MGF of $|\check{h}_{0,k}[t]|^2$ can be expressed as

$$F_{|\check{h}_{0,k}[t]|^2}(w) = e^{-\frac{\mathcal{K}_{0,k}[t]}{2}}\sum_{i=0}^{\infty}\frac{\mathcal{K}_{0,k}^i[t]}{2^i i!}\frac{\gamma\left(1+i, w\check{g}_{0,k}[t]\right)}{\Gamma(1+i)}, \quad (11)$$

and

$$\mathcal{M}_{\left|\check{h}_{0,k}[t]\right|^2}(s) = \frac{\exp\left(\frac{s\,\mathcal{K}_{0,k}[t]}{1-2s}\right)}{(1-2s)}, \quad \text{for} \quad 2s < 1, \quad (12)$$

where $\gamma(a, x)$ is a lower incomplete Gamma function defined as $\gamma(a, x) = \int_0^x e^{-t}t^{a-1}dt$ [44].

Further, as discussed after (6), we have $X_{m_j,k}[t] \sim \mathcal{N}\left(\mathbb{E}[X_{m_j,k}[t]], \mathbb{V}[X_{m_j,k}[t]]\right)$. Therefore, following (9), we can say that $\check{X}_{m_j,k}[t]$ also follows real-valued Gaussian distribution with

$$\begin{aligned}\mathbb{E}[\check{X}_{m_j,k}[t]] &= \varrho_{m_j,k}[t]N\mathbb{E}[X_{m_j,k,n}[t]], \\ \mathbb{V}[\check{X}_{m_j,k}[t]] &= \varrho_{m_j,k}^2[t]N\mathbb{V}[X_{m_j,k,n}[t]] + \varrho_{m_j,k}^2[t]\sigma_{e,k}^2 \\ &\quad + (1-\varrho_{m_j,k}^2[t])\sigma_{d,k}^2, \\ &\triangleq N\mathbb{V}[X_{m_j,k,n}[t]]\left[\varrho_{m_j,k}^2[t](1+\delta_{1,e,k}^2)\right. \\ &\quad \left.+(1-\varrho_{m_j,k}^2[t])\delta_{1,d,k}^2\right], \quad (13)\end{aligned}$$

where $\delta_{1,a,k}^2[t] = \frac{\sigma_{a,k}^2}{N\mathbb{V}[X_{m_j,k,n}[t]]}$, $a \in \{e, d\}$, is the normalized error variance for the composite link at the user, and $\mathbb{E}[X_{m_j,k,n}[t]]$ and $\mathbb{V}[X_{m_j,k,n}[t]]$ are given in (6). If we define $X_{m_j,k}^{'}[t] \triangleq \frac{1}{\sqrt{\mathbb{V}[\check{X}_{m_j,k}[t]]}}\check{X}_{m_j,k}[t]$, we can write $X_{m_j,k}^{'}[t] \sim \mathcal{N}\left(\frac{\mathbb{E}[\check{X}_{m_j,k}[t]]}{\sqrt{\mathbb{V}[\check{X}_{m_j,k}[t]]}}, 1\right)$ and therefore, $\left|X_{m_j,k}^{'}[t]\right|^2$ will follow the NCCS distribution with DoF $= 1$ and non-centrality parameter $\Xi_{m_j,k}[t] = \frac{\mathbb{E}^2[X_{m_j,k}[t]]}{\mathbb{V}[\check{X}_{m_j,k}[t]]}$. The MGF of $\left|X_{m_j,k}^{'}[t]\right|^2$ can be expressed as

$$\mathcal{M}_{\left|X_{m_j,k}^{'}[t]\right|^2}(s) = \frac{\exp\left(\frac{s\,\Xi_{m_j,k}[t]}{1-2s}\right)}{\sqrt{(1-2s)}}, \quad \text{for} \quad 2s < 1. \quad (14)$$

Also, by following [43], we can write the PDF of $|\check{X}_{m_j,k}[t]|^2$ as (15), shown on the top of the next page, where $I_v(\cdot)$ represents the modified Bessel function of first kind [44] and the CDF of $|\check{X}_{m_j,k}[t]|^2$ as

$$\begin{aligned}F_{|\check{X}_{m_j,k}[t]|^2}(x) &= F_{|X_{j,k}^{'}[t]|^2}\left(\frac{x}{\mathbb{V}[\check{X}_{m_j,k}[t]]}\right), \\ &= \exp\left(-\frac{\Xi_{m_j,k}[t]}{2}\right)\sum_{i=0}^{\infty}\frac{\left(\frac{\Xi_{m_j,k}[t]}{2}\right)^i}{i!}\frac{\gamma\left(\frac{1}{2}+i, \frac{x}{2\mathbb{V}[\check{X}_{m_j,k}[t]]}\right)}{\Gamma\left(\frac{1}{2}+i\right)}. \quad (16)\end{aligned}$$

Furthermore, let $\check{X}_k[t] = \sum_{j=1}^{J}|\check{X}_{m_j,k}[t]|^2$, we can then define $\check{X}_k[t]$ as the weighted sum of the J NCCS distributed RVs $\left|X_{m_j,k}^{'}[t]\right|^2$, $j = 1, 2, \ldots, J$, i.e., $\check{X}_k[t] = \sum_{j=1}^{J}u_{j,k}\left|X_{m_j,k}^{'}[t]\right|^2$, where $u_{j,k} = \mathbb{V}[\check{X}_{m_j,k}[t]]$. Thus,

$$f_{|\check{X}_{m_j,k}[t]|^2}(x) = \frac{1}{\mathbb{V}[\check{X}_{m_j,k}[t]]} f_{|X'_{m_j,k}[t]|^2}\left(\frac{x}{\mathbb{V}[\check{X}_{m_j,k}[t]]}\right),$$
$$= \frac{\left(\frac{\Xi_{m_j,k}[t]}{x}\right)^{\frac{1}{4}}}{2\left(\mathbb{V}[\check{X}_{m_j,k}[t]]\right)^{3/4}} \exp\left(-\frac{x}{2\mathbb{V}[\check{X}_{m_j,k}[t]]} - \frac{\Xi_{m_j,k}[t]}{2}\right) I_{-\frac{1}{2}}\left(\sqrt{\frac{\Xi_{m_j,k}[t]x}{\mathbb{V}[\check{X}_{m_j,k}[t]]}}\right), \quad (15)$$

$\check{X}_k[t]$ follows Generalized NCCS distribution with MGF defined as

$$\mathcal{M}_{\check{X}_k[t]}(s) = \prod_{j=1}^{J} \mathcal{M}_{|\check{X}_{m_j,k}[t]|^2}(s) = \prod_{j=1}^{J} \mathcal{M}_{|X'_{m_j,k}[t]|^2}(u_{j,k}s),$$
$$= \prod_{j=1}^{J} \frac{\exp\left(\frac{u_{j,k}s\,\Xi_{m_j,k}[t]}{1-2u_{j,k}s}\right)}{\sqrt{(1-2u_{j,k}s)}},$$
$$= \frac{\exp\left(\sum_{j=1}^{J} \frac{u_{j,k}s\,\Xi_{m_j,k}[t]}{1-2u_{j,k}s}\right)}{\prod_{j=1}^{J}\sqrt{(1-2u_{j,k}s)}}. \quad (17)$$

The PDF of $\check{X}_k[t]$ can be evaluated through MGF as $f_{\check{X}_k[t]}(x) = \frac{1}{2\pi}\int_{-\infty}^{\infty} \mathcal{M}_{\check{X}_k[t]}(-j\omega)e^{j\omega x}d\omega$, however, it does not have tractable closed-form solution for arbitrary $u_{j,k}$, for all $j = 1, 2, \ldots, J$ and $k \in \mathbb{K}$.

Remark 1: *For equal variances of the selected composite channels through the J selected RISs under imperfect and outaded CSI conditions at the k-th user, (i.e., $u_{j,k} = \mathbb{V}[\check{X}_{m_j,k}[t]] = u_k$, for all j), the MGF of $\check{X}_k[t]$ can be given as $\mathcal{M}_{\check{X}_k[t]}(s) = (1-2u_k s)^{-\frac{J}{2}} \exp\left(\frac{u_k\, s\, \Xi_k[t]}{1-2u_k s}\right)$, which reflects that $\check{X}_k[t]$ is a scaled (by a factor of u_k) NCCS distributed RV with DoF J and non-centrality parameter $\Xi_k[t] = \sum_{j=1}^{J} \Xi_{m_j,k}[t]$. Therefore, the PDF of $\check{X}_k[t]$ can be expressed as*

$$f_{\check{X}_k[t]}(x) = \frac{1}{2u_k}\left(\frac{x}{u_k\,\Xi_k[t]}\right)^{\frac{J}{4}-\frac{1}{2}} \exp\left(-\frac{x}{2u_k} - \frac{\Xi_k[t]}{2}\right) \times I_{\frac{J}{2}-1}\left(\sqrt{\frac{\Xi_k[t]x}{u_k}}\right). \quad (18)$$

Further, for $J = 1$, the PDF of $\check{X}_k[t]$ given in (18) is exact with no constraint on weight u_k.

C. Approximate Statistics of Instantaneous SNR under Imperfect and Outdated CSI at User

Let $Z_k[t] \triangleq |\check{h}_{0,k}[t]|^2 + \check{X}_k[t]$, the CDF of $Z_k[t]$ can be evaluated by following [43] as

$$F_{Z_k[t]}(z) = \int_0^z f_{\check{X}_k[t]}(x) F_{|\check{h}_{0,k}[t]|^2}(z-x)dx,$$
$$= \frac{1}{2\pi}\int_0^z \int_{-\infty}^{\infty} \mathcal{M}_{\check{X}_k[t]}(-j\omega)e^{j\omega x} F_{|\check{h}_{0,k}[t]|^2}(z-x)d\omega dx. \quad (19)$$

The integrals in (19) are difficult to solve for arbitrary J due to the complicated MGF expression in (17). However, following the Remark 1, we can rewrite the CDF of $Z_k[t]$ by utilizing (18) and (11) as (20), where $\mathcal{S}_{k,i}(z)$ is defined in (21), shown on the next page. Utilizing infinite series for $\gamma(s,x) = x^s\Gamma(s)e^{-x}\sum_{q=0}^{\infty}\frac{x^q}{\Gamma(s+q+1)}$ and $I_v(x) = \left(\frac{x}{2}\right)^v \sum_{l=0}^{\infty}\frac{\left(\frac{x^2}{4}\right)^l}{l!\Gamma(v+l+1)}$ in (21), followed by the use of [44, Eq. 3.383.1], we get $\mathcal{S}_{k,i}(z)$ given in (22) as shown on the next page, where $\mathcal{B}(a,b)$ and ${}_1\mathcal{F}_1(a;b;x)$ are the Beta and Confluent Hyper-geometric functions, respectively [44]. Substituting (22) in (20), we get the CDF of $Z_k[t]$. The simulated and analytical CDF[3] of $Z_k[t]$ is shown in Fig. 2 for two different values of J with $M = 3$ and $N = 32$. In Fig. 2, we have also shown the impact of imperfect and outdated CSI at k-th user on the CDF.

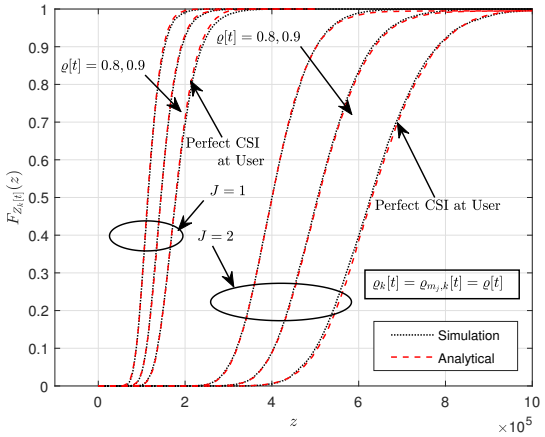

Fig. 2: CDF of $Z_k[t]$ for different values of J with $M = 3$ and $N = 32$.

Remark 2: *It can be observed from Fig. 2 that the analytically obtained CDF values (through (20)) closely follows the exact simulated values for both $J = 1$ and $J = 2$ under both perfect and imperfect CSI conditions at the user. For $J = 2$, following Remark 1, we have considered equal variances of two selected composite channels. It shall be noted that (20) (with the use of (22)) contains three infinite series and the convergence of these infinite series is clear from the analytical plots in Fig.2. The number of summation terms required for the convergence of three series for i, q, and l are only 5, 20, and 30, respectively.*

Furthermore, the CDF of $\check{\Gamma}_k[t]$ (defined in (7)) can be obtained as $F_{\check{\Gamma}_k[t]}(z) = F_{Z_k[t]}\left(\frac{z\sigma_k^2}{J\check{P}_{U,k}[t]}\right)$ and is written as (23), shown on the next page, where

[3]Other simulation parameters are same as defined in Table-I in Section VI with UAV location fixed at $(20, 20, 50)$ for $t = 10$.

$$F_{Z_k[t]}(z) = \frac{1}{2u_k}\left(\frac{1}{u_k\Xi_k[t]}\right)^{\frac{J}{4}-\frac{1}{2}} \exp\left(-\frac{\Xi_k[t]+\mathcal{K}_{0,k}[t]}{2}\right)\sum_{i=0}^{\infty}\frac{(\mathcal{K}_{0,k}[t])^i}{2^i i!}\mathcal{S}_{k,i}(z), \tag{20}$$

$$\mathcal{S}_{k,i}(z) = \int_0^z x^{\frac{J}{4}-\frac{1}{2}}\exp\left(\frac{-x}{2u_k}\right) I_{\frac{J}{2}-1}\left(\sqrt{\frac{\Xi_k[t]x}{u_k}}\right)\frac{\gamma\left(1+i,(z-x)\check{g}_{0,k}[t]\right)}{\Gamma(1+i)}dx. \tag{21}$$

$$\begin{aligned}\mathcal{S}_{k,i}(z) =& e^{-\check{g}_{0,k}[t]z}\sum_{q=0}^{\infty}\sum_{l=0}^{\infty} z^{i+q+l+1+\frac{J}{2}}\frac{(\check{g}_{0,k}[t])^{i+q+1}}{(i+q+1)!}\frac{\mathcal{B}\left(i+q+2,\frac{J}{2}+l\right)}{l!\,\Gamma(\frac{J}{2}+l)}\\ &\times\left(\frac{\Xi_k[t]}{4u_k}\right)^{\frac{J}{4}-\frac{1}{2}+l}{}_1\mathcal{F}_1\left(\frac{J}{2}+l;i+q+l+2+\frac{J}{2};\left(\check{g}_{0,k}[t]-\frac{1}{2u_k}\right)z\right),\end{aligned} \tag{22}$$

$$\begin{aligned}F_{\check{\Gamma}_k[t]}(z) =& \Phi_k[t]\exp\left(\frac{-\check{g}_{0,k}[t]\sigma_k^2 z}{J\tilde{P}_{U,k}[t]}\right)\sum_{i=0}^{\infty}\sum_{q=0}^{\infty}\sum_{l=0}^{\infty}\Psi_{k,i,q,l}[t]\left(\frac{z\sigma_k^2}{J\tilde{P}_{U,k}[t]}\right)^{i+q+l+1+\frac{J}{2}}\\ &\times{}_1\mathcal{F}_1\left(\frac{J}{2}+l;i+q+l+2+\frac{J}{2};\left(\check{g}_{0,k}[t]-\frac{1}{2u_k}\right)\left(\frac{z\sigma_k^2}{J\tilde{P}_{U,k}[t]}\right)\right),\end{aligned} \tag{23}$$

$$\begin{aligned}\Phi_k[t] &= \left(\frac{1}{2u_k}\right)^{\frac{J}{2}}\exp\left(-\frac{\Xi_k[t]+\mathcal{K}_{0,k}[t]}{2}\right),\\ \Psi_{k,i,q,l}[t] &= \frac{(\mathcal{K}_{0,k}[t])^i}{2^i i!}\frac{(\check{g}_{0,k}[t])^{i+q+1}}{(i+q+1)!}\\ &\quad\times\frac{\mathcal{B}\left(i+q+2,\frac{J}{2}+l\right)}{l!\,\Gamma(\frac{J}{2}+l)}\left(\frac{\Xi_k[t]}{4u_k}\right)^l.\end{aligned} \tag{24}$$

The CDF of SNR obtained in (23) will be used in the later sections to evaluate the system performance.

IV. Selection of RISs with Imperfect and Outdated CSI at UAV

In this section, we consider the selection of the best $J(<M)$ RISs based on the quality of the composite UAV-RIS-User channels. We also consider that due to the mobility of the UAV and the time varying nature of the channel, the CSI received at the UAV in a given time slot is delayed and hence becomes outdated. Furthermore, there may be errors while estimating the composite channel coefficients. Considering both the outdated and imperfect CSI of composite UAV-RIS$_m$-User$_k$ channels at the UAV (similar to (9) at k-th user), we can write

$$\check{X}_{m,k}[t] = \varrho_u[t]X_{m,k}[t] + \varrho_u[t]X_e[t] + \sqrt{1-\varrho_u^2[t]}X_d[t], \tag{25}$$

where $X_e[t]\sim\mathcal{N}(0,\sigma_{e,u}^2)$ denotes the estimation error value and $X_d[t]\sim\mathcal{N}(0,\sigma_{d,u}^2)$ represents the error term due to the transmission and processing delay. The variable $\varrho_u[t]$ is the correlation coefficient between the estimated and outdated CSIs at UAV in t-th time slot. For a delay of $\tau_{d,u}[t]$, we can write $\varrho_u[t]=\mathcal{J}_0(2\pi f_{d,u}[t]\tau_{d,u}[t])$, with $f_{d,u}[t]$ being the Doppler spread due to the movement of the transceivers.

Practically, the outdated CSI given in (25), for $m\in\mathbb{M}$, is utilized by the UAV to select the best J RISs having the maximum channel gain of the composite UAV-RIS-User channels in a given time slot. It may be noted that the there will be $L=\binom{M}{J}$ different combinations of selecting J RISs among total M RISs. Thus, the probability of selecting J RISs with ℓ-th combination, $\ell=1,2,\ldots,L$, during δ_t can be calculated as (26), shown on the top of the next page, where $\Pr\{\cdot\}$ represents the probability of an event. Similar to (13), we can write $\check{X}_{m,k}[t]\sim\mathcal{N}\left(\mathbb{E}[\check{X}_{m,k}[t]],\mathbb{V}[\check{X}_{m,k}[t]]\right)$, where

$$\begin{aligned}\mathbb{E}[\check{X}_{m,k}[t]] &= \varrho_u[t]N\mathbb{E}[X_{m,k,n}[t]],\\ \mathbb{V}[\check{X}_{m,k}[t]] &= N\mathbb{V}[X_{m,k,n}[t]]\left[\varrho_u^2[t](1+\delta_{e,u}^2[t])\right.\\ &\quad\left.+(1-\varrho_u^2[t])\delta_{d,u}^2[t]\right],\end{aligned} \tag{27}$$

where $\delta_{a,u}^2[t]=\frac{\sigma_{a,u}^2}{N\mathbb{V}[X_{m,k,n}[t]]}$, $a\in\{e,d\}$, is the normalized error variance of the composite fading channel at the UAV. Also, $\mathbb{E}[X_{m,k,n}[t]]$ and $\mathbb{V}[X_{m,k,n}[t]]$ can be obtained from (6) by using $m_j=m$. Thus, the CDF of $|\check{X}_{m,k}[t]|^2$ can be written similar to (16) as

$$\begin{aligned}F_{|\check{X}_{m,k}[t]|^2}(x) &= \exp\left(-\frac{\check{\Xi}_{m,k}[t]}{2}\right)\\ &\quad\times\sum_{i=0}^{\infty}\frac{\left(\frac{\check{\Xi}_{m,k}[t]}{2}\right)^i}{i!}\frac{\gamma\left(\frac{1}{2}+i,\frac{x}{2\mathbb{V}[\check{X}_{m,k}[t]]}\right)}{\Gamma\left(\frac{1}{2}+i\right)},\end{aligned} \tag{28}$$

where $\check{\Xi}_{m,k}[t]=\frac{\varrho_u^2[t]\mathbb{E}^2[X_{m,k}[t]]}{\mathbb{V}[\check{X}_{m,k}[t]]}$. Adopting the similar approach, the PDF of $|\check{X}_{m_j,k}[t]|^2$ can be written similar to (15) as

$$\begin{aligned}f_{|\check{X}_{m_j,k}[t]|^2}(x) =& \frac{1}{2\left(\mathbb{V}[\check{X}_{m_j,k}[t]]\right)^{3/4}}\\ &\times\exp\left(-\frac{x}{2\mathbb{V}[\check{X}_{m_j,k}[t]]}-\frac{\check{\Xi}_{m_j,k}[t]}{2}\right)\\ &\times\left(\frac{\check{\Xi}_{m_j,k}[t]}{x}\right)^{\frac{1}{4}}I_{-\frac{1}{2}}\left(\sqrt{\frac{\check{\Xi}_{m_j,k}[t]x}{\mathbb{V}[\check{X}_{m_j,k}[t]]}}\right),\end{aligned} \tag{29}$$

$$p_{\ell,k}[t] = \Pr\left\{\min\left(|\check{X}_{m_1,k}[t]|^2, |\check{X}_{m_2,k}[t]|^2, \ldots, |\check{X}_{m_J,k}[t]|^2\right) > \max_{\substack{m\in\mathbb{M}\\ m\neq m_1,\ldots,m_J}} \left(|\check{X}_{m,k}[t]|^2\right)\right\},$$
$$= \prod_{j=1}^{J} \Pr\left\{|\check{X}_{m_j,k}[t]|^2 > \max_{\substack{m\in\mathbb{M}\\ m\neq m_1,\ldots,m_J}} \left(|\check{X}_{m,k}[t]|^2\right)\right\},$$
$$= \prod_{j=1}^{J}\left[\int_0^\infty \left(\prod_{\substack{m=1\\ m\neq m_1,\ldots,m_J}}^{M} F_{|\check{X}_{m,k}[t]|^2}(w)\right) f_{|\check{X}_{m_j,k}[t]|^2}(w)dw\right] \triangleq \prod_{j=1}^{J} p_{j,\ell,k}[t], \tag{26}$$

where $\check{\Xi}_{m_j,k}[t] = \frac{\varrho_u^2[t]\mathbb{E}^2[X_{m_j,k}[t]]}{\mathbb{V}[\check{X}_{m_j,k}[t]]}$. Using (29) and (28) in (26), we can evaluate the probability of selecting J RISs under imperfect and outdated CSI of the composite channel.

Remark 3: *It is clear from* (26) *that calculation of $p_{j,\ell,k}[t]$ requires to solve an infinite integral containing a product of $(M-J)$ CDF terms. Moreover, each CDF term involves an infinite series along with the mean and variances obtained through the CLT approximation. Thus, the analytically obtained values of RIS selection probability may deviate from the exact values for lower values of N*

It is noteworthy that obtaining a closed-form expression for (26) is extremely difficult. Therefore, we consider a special case where $J = M-1$ and derive the series based expression for the RIS selection probability as given in following Lemma.

Lemma 1. *For $J = M-1$, the probability $p_{j,\ell,k}[t]$, defined in* (26)*, can be evaluated as*

$$p_{j,\ell,k}[t] = \exp\left(-\frac{\check{\Xi}_{m,k}[t]}{2} - \frac{\check{\Xi}_{m_j,k}[t]}{2}\right) \frac{\left(\check{\Xi}_{m_j,k}[t]\right)^{\frac{1}{4}}}{2\left(\mathbb{V}[\check{X}_{m_j,k}[t]]\right)^{\frac{3}{4}}}$$
$$\times \sum_{i=0}^{\infty}\sum_{q=0}^{\infty} \frac{\left(\check{\Xi}_{m,k}[t]\right)^{i}}{2^i\, i!\left(i+q+\frac{1}{2}\right)!\left(2\mathbb{V}[\check{X}_{m,k}[t]]\right)^{i+q+\frac{1}{2}}} \mathcal{Y}_{i,q,j,k}[t], \tag{30}$$

where $\mathcal{Y}_{i,q,j,k}[t]$ is defined in (31)*, shown on the next page, with $\mathcal{M}_{u,v}(\cdot)$ representing the Whittaker function [44].*

Proof: Assuming that RIS_m is the only RIS which is not being selected, we apply $J = M-1$ in (26). Further, using infinite series of lower incomplete gamma function as $\gamma(s,x) = x^s\Gamma(s)e^{-x}\sum_{q=0}^{\infty}\frac{x^q}{\Gamma(s+q+1)}$ [44] in (28) along with the use of (29), and subsequently utilizing [44, Eq. 6.643.2], we get (30). ∎

V. Performance Analysis

In this section, we analyze the performance of the considered UAV-based RIS-assisted multiuser downlink communication system in terms of average coverage probability (ACP) and average bit-error-rate (ABER) over complete flying duration of the UAV. The expressions for these performance matrices have been obtained under the imperfect and outdated CSI (both at the user and the UAV) of the composite as well as direct channel with RIS selection adopted by the UAV.

A. Average Coverage Probability Analysis

The coverage probability for a ground user under the considered multi-user downlink communication network is defined as the probability that the instantaneously received SNR at k-th user in t-th time slot exceeds a predefined threshold SNR as per the Quality-of-Service (QoS) requirements of the user. If the k-th user receives the signal through direct link and J RISs (with ℓ-th combination), mathematically, we may formulate the coverage probability under imperfect and outdated CSI conditions during t-th time slot as

$$\mathcal{P}_{\text{Cov}}(\ell,k,t;\Gamma_{\text{Th}}) = \Pr\{\check{\Gamma}_k[t] \geq \Gamma_{\text{Th}}\} = 1 - F_{\check{\Gamma}_k[t]}(\Gamma_{\text{Th}}), \tag{32}$$

where Γ_{Th} is the predefined threshold SNR and the CDF of $\check{\Gamma}_k[t]$ is defined in (23), which includes the impact of imperfect and outdated CSI at the k-th user. Considering all possible combinations of J RISs, the ACP at k-th user under imperfect and outdated CSI based RIS selection scheme can be evaluated for total flight duration as

$$\mathcal{P}_{\text{Cov}}(k;\Gamma_{\text{Th}}) = \frac{1}{T}\sum_{t=1}^{T}\sum_{\ell=1}^{L} p_{\ell,k}[t]\mathcal{P}_{\text{Cov}}(\ell,k,t;\Gamma_{\text{Th}}), \tag{33}$$

where $p_{\ell,k}[t]$ is the selection probability of ℓ-th combination of J RISs, as given in (26).

Lemma 2. *For low values of transmit power available at UAV in a given time slot for k-th ground user (i.e., $\tilde{P}_{U,k}[t] \to 0$), the coverage probability can be asymptotically expressed as* (34)*, shown on the next page, where*

$$\mathcal{D}_1(k,i,q,l,t;\Gamma_{Th}) = \frac{\Gamma\left(i+q+l+2+\frac{J}{2}\right)}{\check{g}_{0,k}[t]\Gamma(i+q+2)}$$
$$\times\left(\frac{1}{2u_k} - \check{g}_{0,k}[t]\right)^{-\frac{J}{2}-l}\left(\frac{\Gamma_{Th}\sigma_k^2}{J}\right)^{i+q},$$
$$\mathcal{D}_2(k,i,q,l,t;\Gamma_{Th}) = \frac{2u_k\Gamma\left(i+q+l+2+\frac{J}{2}\right)}{\Gamma\left(\frac{J}{2}+l\right)}$$
$$\times\left(\check{g}_{0,k}[t] - \frac{1}{2u_k}\right)^{-i-q-2}\left(\frac{\Gamma_{Th}\sigma_k^2}{J}\right)^{\frac{J}{2}+l-2}. \tag{35}$$

Proof: Utilizing the asymptotic expression of hypergeometric function for large argument as $\lim_{z\to\infty}{}_1\mathcal{F}_1(a,b;z) \propto \frac{\Gamma(b)}{\Gamma(b-a)}(-z)^{-a} + \frac{\Gamma(b)}{\Gamma(a)}e^z(-z)^{a-b}$, [45, 07.20.06.0009.01] alongside $\lim_{z\to\infty} e^{-az} \approx \frac{1}{az}$ in (23), and substituting the

$$\mathcal{Y}_{i,q,j,k}[t] = \frac{2(i+q)!}{\sqrt{\pi}} \left(\frac{2\mathbb{V}[\check{X}_{m,k}[t]]\mathbb{V}[\check{X}_{m_j,k}[t]]}{\mathbb{V}[\check{X}_{m,k}[t]] + \mathbb{V}[\check{X}_{m_j,k}[t]]} \right)^{i+q+\frac{3}{4}} \exp\left(\frac{\check{\Xi}_{m_j,k}[t]\mathbb{V}[\check{X}_{m,k}[t]]}{4(\mathbb{V}[\check{X}_{m,k}[t]] + \mathbb{V}[\check{X}_{m_j,k}[t]])} \right) \times \sqrt{\frac{\mathbb{V}[\check{X}_{m_j,k}[t]]}{\check{\Xi}_{m_j,k}[t]}} \mathcal{M}_{-(i+q+\frac{3}{4}),-\frac{1}{4}} \left(\frac{\check{\Xi}_{m_j,k}[t]\mathbb{V}[\check{X}_{m,k}[t]]}{2(\mathbb{V}[\check{X}_{m,k}[t]] + \mathbb{V}[\check{X}_{m_j,k}[t]])} \right), \tag{31}$$

$$\mathcal{P}^{\infty}_{\text{Cov}}(\ell,k,t;\Gamma_{\text{Th}}) \propto 1 - \Phi_k[t] \sum_{i=0}^{\infty}\sum_{q=0}^{\infty}\sum_{l=0}^{\infty} \Psi_{k,i,q,l}[t] \left[\frac{\mathcal{D}_1(k,i,q,l,t;\Gamma_{\text{Th}})}{\left(\tilde{P}_{U,k}[t]\right)^{i+q}} + \frac{\mathcal{D}_2(k,i,q,l,t;\Gamma_{\text{Th}})}{\left(\tilde{P}_{U,k}[t]\right)^{\frac{J}{2}+l-2}} \right], \tag{34}$$

resulting asymptotic CDF in (32) with some algebraic manipulations, we get (34). ∎

The purpose of assuming the low transmit power conditions on Lemma 2 is to observe the analytical behavior of derived ACP expression for sufficiently low transmit power available at UAV in a given time slot. In general, UAV is a power constrained source and it is possible over a given time slot that the power allocated to a particular user (especially in a large user setup) goes very low. In that case, as discussed in Lemma 2, the coverage probability drops very quickly for a small change in the transmit power values. The same behavior can also be observed through Fig. 3. Moreover, it can be noted form the results of Lemma 2 that term $\mathcal{D}_p(k,i,q,l,t;\Gamma_{\text{Th}})$, $p=1,2$ in (35) depends upon $\check{g}_{0,k}[t]$ and u_k, and it is clear from the discussion in Subsection III-B that $\check{g}_{0,k}[t]$ and u_k are functions of imperfect and outdated CSI parameters of direct and composite channels, respectively, between the UAV and the k-th user.

B. Average Bit-Error-Rate Analysis

Now, we focus on deriving a unified closed-form expression of average BER of the k-th user for different binary modulation schemes such as binary phase shift keying (BPSK), binary frequency shift keying (BFSK), and differential phase shift keying (DPSK).

Lemma 3. *The unified ABER at k-th user in t-th time slot for the considered communication system with J out of M RISs selected by the UAV (in ℓ-th combination) is given as* (36)*, shown on the next page, where $\mathcal{A}_{i,q,l}(\ell,k,t)$ is defined as* (37)*, shown on the next page, with $(\cdot)_s$ denoting the Pochhammer symbol. The parameters (a,b) corresponds to the binary modulation scheme, such as $(0.5,1)$ for BPSK, $(1,1)$ for DPSK, and $(0.5,0.5)$ for BFSK.*

Proof: The unified BER (for different binary modulation format) at k-th user in t-th time slot can be evaluated as [46, Eq. 12]

$$\mathcal{P}_{\text{E}}(\ell,k,t) = \frac{b^a}{2\Gamma(a)} \int_0^{\infty} \exp(-b\gamma)\gamma^{a-1} F_{\check{\Gamma}_k}[t](\gamma) d\gamma. \tag{38}$$

Using the CDF $F_{\check{\Gamma}_k[t]}(\gamma)$ from (23) along with the utilization of the series expansion ${}_1\mathcal{F}_1(a_0;b_0;z) = \sum_{s=0}^{\infty} \frac{(a_0)_s z^s}{(b_0)_s s!}$, and applying [44, Eq. 3.351.3], we get (36). ∎

Thus, the ABER at k-th user over complete flight duration of the UAV under imperfect and outdated CSI based RIS selection scheme can be evaluated as

$$\mathcal{P}_{\text{E}}(k) = \frac{1}{T} \sum\nolimits_{t=1}^{T} \sum\nolimits_{\ell=1}^{L} p_{\ell,k}[t] \mathcal{P}_{\text{E}}(\ell,k,t), \tag{39}$$

where $\mathcal{P}_{\text{E}}(\ell,k,t)$ is defined in (36).

Lemma 4. *For high transmit power conditions at UAV (i.e., $\tilde{P}_{U,k}[t] \to \infty$), the BER at k-th user in t-th time slot can be written as*

$$\mathcal{P}^{\infty}_{E}(\ell,k,t) \propto \left(\frac{1}{\tilde{P}_{U,k}[t]} \right)^{\frac{J}{2}+1} \tag{40}$$

Proof: Considering the hypergeometric function for small argument as $\lim_{z\to 0} {}_1\mathcal{F}_1(a,b;z) \approx 1$, [45, 07.20.06.0001.02] in (23), substituting the resulting CDF in (38), and solving the integral, we get

$$\mathcal{P}^{\infty}_{\text{E}}(\ell,k,t) = \frac{\Phi_k[t]}{2\Gamma(a)} \sum_{i=0}^{\infty}\sum_{q=0}^{\infty}\sum_{l=0}^{\infty} \Psi_{k,i,q,l}[t] \left(\frac{\sigma_k^2}{J\tilde{P}_{U,k}[t]} \right)^{i+q+l+1+\frac{J}{2}}. \tag{41}$$

For high values of transmit power ($\tilde{P}_{U,k}[t] \to \infty$), the term with $i=q=l=0$ will dominate the summation in (41). Using this fact, we get (40). ∎

It can be observed from Lemma 4 that for very large values of $\tilde{P}_{U,k}[t]$, the rate of decay in ABER values depends upon the number of selected RISs by the UAV.

VI. Numerical Results and Discussions

This section presents the simulated and analytical performances of ACP and ABER for the considered RIS-assisted UAV based multiuser communication network with the RIS selection under outdated and imperfect CSIs at the user as well as the UAV. Table I shows the important variables and their values used for obtaining the numerical results in this section. The operating frequency of downlink UAV-assisted communication is assumed as 2.4 GHz (i.e., $\lambda = 0.125$ m) as it is an approved frequency of operation for unmanned aircraft systems. In practical systems, it can be used as the backup frequency of remote control uplink, telemetry downlink, and information transmission link. For practical assumptions, we have considered all the link distances between $30-80$ meters.

$$\mathcal{P}_{\mathrm{E}}(\ell,k,t)=\frac{b^a\Phi_k[t]}{2\Gamma(a)}\sum_{i=0}^{\infty}\sum_{q=0}^{\infty}\sum_{l=0}^{\infty}\left(\frac{\sigma_k^2}{J\tilde{P}_{U,k}[t]}\right)^{i+q+l+1+\frac{J}{2}}\Psi_{k,i,q,l}[t]\mathcal{A}_{i,q,l}(\ell,k,t), \tag{36}$$

$$\mathcal{A}_{i,q,l}(\ell,k,t)=\sum_{s=0}^{\infty}\frac{(\frac{J}{2}+l)_s\,\left(a+i+q+l+s+\frac{J}{2}\right)!}{\left(i+q+l+2+\frac{J}{2}\right)_s\,s!\left(\frac{J\tilde{P}_{U,k}[t]}{\sigma_k^2}\right)^s}\frac{\left(\breve{g}_{0,k}[t]-\frac{1}{2u_k}\right)^s}{\left(b+\frac{\sigma_k^2\breve{g}_{0,k}[t]}{J\tilde{P}_{U,k}[t]}\right)^{a+i+q+l+s+1+\frac{J}{2}}}, \tag{37}$$

TABLE I: List of some important variables and their values taken for numerical results.

Variable	Value	Variable	Value	Variable	Value	Variable	Value
$\boldsymbol{\chi}_1$	$(25,25,0)$	$\varrho_u[t]$	0.8	$\boldsymbol{\chi}_{R_1}$	$(25,30,30)$	$\boldsymbol{\chi}_U[0]$	$(0,0,50)$
$\boldsymbol{\chi}_2$	$(17,17,0)$	σ_k^2	1	$\boldsymbol{\chi}_{R_2}$	$(15,10,30)$	$\boldsymbol{\chi}_U[25]$	$(50,50,50)$
$\boldsymbol{\chi}_3$	$(33,33,0)$	$\Lambda_{m,k}$	1	$\boldsymbol{\chi}_{R_3}$	$(35,30,30)$	H_U	50 m
$\boldsymbol{\chi}_4$	$(9,9,0)$	β	2	$\boldsymbol{\chi}_{R_4}$	$(5,10,30)$	$\rho_{m,n}[t]$	1
$\boldsymbol{\chi}_5$	$(41,41,0)$	$\Omega_{0,k}=\Omega_m$	1	$\boldsymbol{\chi}_{R_5}$	$(45,50,30)$	$\mu_{0,k}[t]$	$1+1j$
$\lvert\mu_m[t]\rvert$	1.8	$\lvert\nu_{m,k}\rvert$	1.12	T	25	T_C	5 sec.

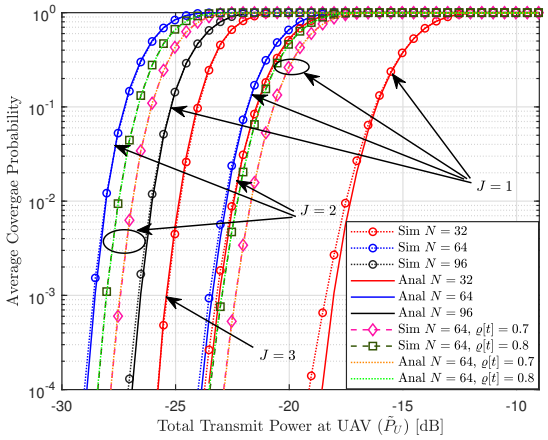

Fig. 3: ACP versus UAV transmit power performance of User-1 located at $(25,25,0)$ for different values of N, J with $M=5$.

It is assumed here that all the RISs available in the network have same size (i.e., N). A propulsion power of 24 dB is assumed following the parameters in [41]. It is also assumed that the movement of UAV over horizontal $X-Y$ plane is linear and the speed of motion is 14.14 m/s for all the time slots. For majority of results shown in this section, we have considered User-1 with 3D coordinate fixed at $(25,25,0)$, however, the derived results are applicable for any arbitrary user location coordinate in the 3-D coordinate system. For $M=5$, the locations of all 5 RISs are given in Table I, however, for any other value of M, the 3D coordinate of RIS location are explicitly specified in the figure caption as simulation parameters. The simulations are performed over 10^5 iterations. Unless mentioned specifically, the curves shown in this section are valid for $\varrho_{0,k}[t]=\varrho_{m_j,k}[t]=1$ and $\delta^2_{0,e,k}[t]=\delta^2_{1,e,k}[t]=0$.

A. Results for ACP

Fig. 3 shows the variations of the ACP of User-1 with respect to (w.r.t.) the total transmit power available at the UAV for $M=5$ and different values of N, J. First we assume the outdated and imperfect CSI conditions at UAV only such that the probability of RIS selection is affected due to the same. For that, we have considered $\sigma^2_{d,u}=\sigma^2_{e,u}=0.1$ and $\varrho_u[t]=0.8$. It can be observed from Fig. 3 that the coverage performance of User-1 significantly improves with increasing N (for a given value of J). Moreover, the ACP performance of User-1 improves for increasing J (with fixed N), however the performance gain after every single increase in J reduces. For example, with $N=32$ and an ACP value of 0.1, selecting one RIS out of total 5 (i.e., $J=1$) requires a total transmit power of approx -16.25 dB, whereas for $J=2$ and $J=3$, the total power requirement at UAV reduces to nearly -21.5 dB and -24 dB, respectively. Thus, the performance gain for increasing J from 1 to 2 is higher than that for 2 to 3. Further, it can be noticed from Fig. 3 that the gap (due to the NCCS approximation) between the analytical and simulated ACP curves decreases for higher value of N as well as J.

Observation 1: *It is interesting to observe from Fig. 3 that the ACP of User-1 for $(N,J)=(64,1)$ is higher as compared to that for $(N,J)=(32,2)$. Similarly, the ACP performance of a user served through a single selected RIS with $N=96$ is superior than that under three RIS selection ($J=3$) with $N=32$. It should be noted that for the two scenarios mentioned above, the product NJ remains constant, which reflects the total number of reflecting elements utilized for the communication. Moreover, the performance gain is higher for large vale of product NJ. Thus, it can deduced that selecting more RISs from a group of small-sized RISs may not be as good as selecting fewer RISs from a group of large-sized RISs.*

Further, we have also plotted the ACP performance of User-1 under the imperfect and outdated CSI conditions of direct as well as composite channel at the user as well. For this, we have assumed $\varrho_{0,k}[t]=\varrho_{m_j,k}[t]=\varrho[t]$ and have taken two different values of $\varrho[t]$ as 0.7 and 0.8. We have also assumed that error variances for outdated and imperfect CSI at the user are same as that considered at UAV. It can be observed from Fig. 3 that ACP performance deteriorates further for an imperfect and outdated CSI conditions at the User itself. Moreover, lower

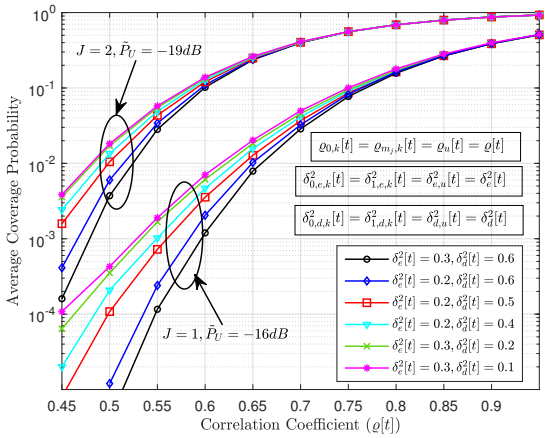

Fig. 4: Variations of ACP performance of User-1 w.r.t. correlation coefficient ($\varrho[t]$) for outdated CSI under different settings of normalized error variances $\delta^2_d[t]$, $\delta^2_e[t]$ with $M = 3$, $N = 32$ and varying values of $\tilde{P}_U$, J. The 3D locations of three RISs are considered as $\boldsymbol{\chi}_{R_1}$, $\boldsymbol{\chi}_{R_2}$, and $\boldsymbol{\chi}_{R_3}$.

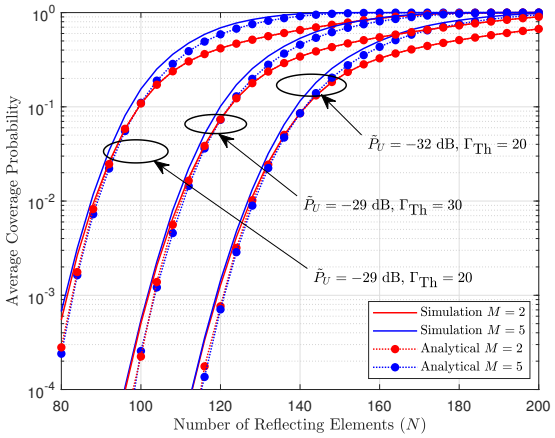

Fig. 5: Variations of ACP of User-1 w.r.t. N for varying M, $\tilde{P}_U$, and Γ_{Th} under negligible estimation error at UAV (i.e., $\delta^2_{e,u}[t] = 0.01$) and high correlation coefficient at UAV (i.e., $\varrho_u[t] = 0.95$). For $M = 2$, the RISs are located at $\boldsymbol{\chi}_{R_1}$ and $\boldsymbol{\chi}_{R_2}$.

the correlation between estimated and outdated CSI at the user, poorer the ACP performance of the user for all values J.

In Fig. 4, we investigate the impact of outdated and imperfect CSI parameters on the analytical ACP performance of the considered network with $M = 3$ and $N = 32$. For the curves in Fig. 4, the 3D locations of the RISs are considered as $\boldsymbol{\chi}_{R_1}$, $\boldsymbol{\chi}_{R_2}$, and $\boldsymbol{\chi}_{R_3}$. For this, we have assumed equal parameters for imperfect and outdated CSIs at both UAV and the user, i.e., we have assumed (i) $\delta^2_{0,e,k}[t] = \delta^2_{1,e,k}[t] = \delta^2_{e,u}[t] = \delta^2_e[t]$ (say), (ii) $\delta^2_{0,d,k}[t] = \delta^2_{1,d,k}[t] = \delta^2_{d,u}[t] = \delta^2_d[t]$ (say), and (iii) $\varrho_{0,k}[t] = \varrho_{m_j,k}[t] = \varrho_u[t] = \varrho[t]$ (say), for all $t \in \mathbb{T}$. We have plotted the ACP values of User-1 w.r.t. the correlation coefficient ($\varrho[t]$) for different values of J, $\tilde{P}_U$, $\delta^2_e[t]$, and $\delta^2_d[t]$. It can be observed from Fig. 4 that for large values of $\varrho[t]$, the coverage performance of User-1 is very high under all the values of normalized error variances considered in the figure. However, under moderate and low values of $\varrho[t]$, the impact of error variances is significant under all the values of J and $\tilde{P}_U$ considered here.

Observation 2: *It may be noticed from Fig. 4 that for $\varrho[t] = 0.5$ and $\delta^2_e[t] = 0.2$, the ACP values of User-1 under $J = 1$ reduces by almost 10 times with an increase in $\delta^2_d[t]$ from 0.5 to 0.6. Whereas, for the same increase in $\delta^2_d[t]$, the ACP under $J = 2$ reduces by almost 2 times. Thus, it can be deduced that selecting more RISs can provide better gains under outdated and imperfect CSI conditions. Furthermore, it can be seen from Fig. 4 that for $J = 2$, the ACP performance of User-1 is almost unchanged (under various settings of normalized error variances) for $\varrho[t] \geq 0.65$, whereas for $J = 1$, the similar behavior is observed for $\varrho[t] \geq 0.85$ only.*

In Fig. 5, we have shown the variations of ACP of User-1 located at $(25, 25, 0)$ w.r.t. the number of RIS reflecting elements for different values of M, $\tilde{P}_U$ and Γ_{Th}. For this figure, we have considered sufficiently large correlation coefficient for outdated CSI and negligible channel estimation error. In order to observe the impact of M, we have fixed $J = 1$. It shall be noted that For $M = 2$, we have considered RISs with 3D locations $\boldsymbol{\chi}_{R_1}$ and $\boldsymbol{\chi}_{R_2}$. Moreover, the curves in Fig. 5 are valid for $\varrho_{0,k}[t] = \varrho_{m_j,k}[t] = 1$ and $\delta^2_{0,e,k}[t] = \delta^2_{1,e,k}[t] = 0$.

Observation 3: *It can be observed from Fig. 5 that putting more RISs in the network may not necessarily provide significant ACP performance improvement for a given N. Actually, it is the size of the RISs available in the network which plays a deciding role in calculating the amount of achievable performance improvement. For a particular range of N, we can observe significant improvement in the ACP performance with more RISs, however, the ACP values for different M remain almost same outside that range. For example, with $\tilde{P}_U = -29$ dB and $\Gamma_{Th} = 20$, if the UAV selects one out of all 5 RISs considered in the setup with $N = 120$ at each RIS, the ACP value of User-1 is nearly 0.7 as compared to an ACP value of approximately 0.4 when UAV selects one out of two RISs (located at $\boldsymbol{\chi}_{R_1}$ and $\boldsymbol{\chi}_{R_2}$) having same size. However, if we reduce the number of reflecting elements at each RIS to $N = 100$, User-1 gets an ACP of 0.15 and 0.1 under single RIS selection out of $M = 5$ and $M = 2$, respectively, keeping all other system parameters fixed.*

Moreover, the range of interest for N varies with system parameters like $\tilde{P}_U$ and Γ_{Th}. For $\tilde{P}_U = -29$ dB and $\Gamma_{\text{Th}} = 20$, choosing N between 100 to 150 provides significant performance improvement with $M = 5$ as compared to $M = 2$. However, for $\tilde{P}_U = -29$ dB and $\Gamma_{\text{Th}} = 30$, the similar gains may be achieved by choosing N between 120 to 190. Thus, decreasing transmit power and/or increasing threshold SNR require larger-sized RISs to achieve a given ACP performance.

Fig. 6 shows variations of ACP for User-1, User-4, and User-5, located at $\boldsymbol{\chi}_1$, $\boldsymbol{\chi}_4$, and $\boldsymbol{\chi}_5$, respectively, in a 5-user setup. For the curves in Fig. 6, we have set $\varrho_{0,k}[t] = \varrho_{m_j,k}[t] = 1$, $\delta^2_{0,e,k}[t] = \delta^2_{1,e,k}[t] = 0$, and $\delta^2_{e,u}[t] = \delta^2_{d,u}[t] = 0.1$. It can be clearly noticed from Fig. 6 that the ACP performance of User-4 and User-5 (which are located at the two extremes of the horizontal X-Y plane covered by the UAV flight) is significantly improved by increasing the number of RISs available in the network for both the values of $\varrho_u[t]$ considered in the figure. However, the ACP performance of User-1 (located in the center of the horizontal plane under consideration) is almost unaffected (very small improvement

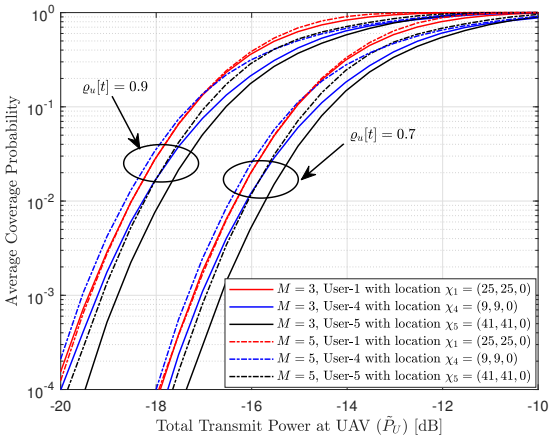

Fig. 6: ACP versus UAV transmit power performance for different user locations with $N = 32$, $J = 1$, $\varrho_u[t] = 0.7, 0.9$, and $M = 3, 5$. For $M = 3$, the 3D locations of the RISs are considered as $\boldsymbol{\chi}_{R_1}$, $\boldsymbol{\chi}_{R_2}$, and $\boldsymbol{\chi}_{R_3}$.

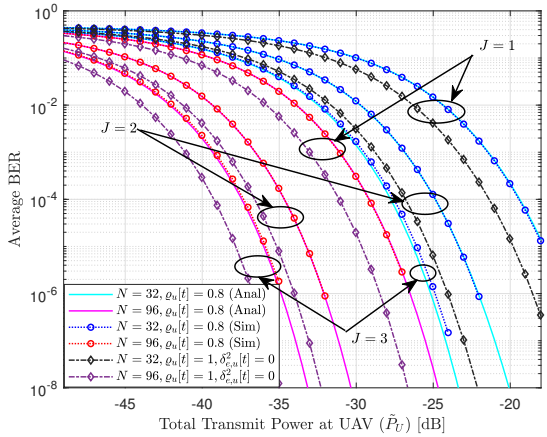

Fig. 7: ABER versus transmit power performance of User-1 with $M = 3$, and varying values of N, J under for BPSK modulation scheme. The three RISs are assumed to be located at $\boldsymbol{\chi}_{R_1}$, $\boldsymbol{\chi}_{R_2}$, and $\boldsymbol{\chi}_{R_3}$.

is observed at higher values of transmit power) by increasing M from 3 to 5. It can also be seen from Fig. 6 that for $M = 3$, the user at the centre location i.e., $(25, 25, 0)$ outperform the other users in terms of ACP performance for all values of transmit power considered in the figure, however, for $M = 5$, User-4 with 3D location $(9, 9, 0)$ performs slightly better than User-1 upto certain value of transmit power beyond which User-1 takes over with a significant margin.

B. Results for ABER

Fig. 7 shows the average BER performance of a ground user at location $(25, 25, 0)$ in the considered network w.r.t. total transmit power available at UAV under imperfect and outdated CSI based RIS selection schemes. We have considered BPSK modulation scheme with $M = 3$, $J = 1, 2, 3$, and $N = 32, 96$. For imperfect CSI at UAV, we have taken $\delta^2_{e,u}[t] = 0.1$ and for outdated CSI at UAV, we have assumed $\delta^2_{d,u}[t] = 0.1$, $\varrho_u[t] = 0.8$. It is clear from Fig. 7 that the ABER performance of User-1 enhances significantly by increasing J and N. However, the performance gain due to an increase in J (for fixed N) reduces

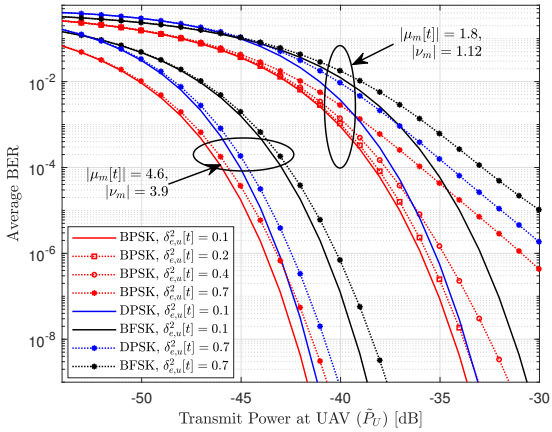

Fig. 8: ABER versus transmit power performance of User-1 for different binary modulation schemes with $M = 5$, $N = 96$, $J = 3$, $\varrho_u[t] = 0.8$ and $\delta^2_{d,u}[t] = 0.1$ under different values of $\delta^2_{e,u}[t]$, $|\mu_m[t]|$, and $|\nu_m|$.

with J. For example, to get an ABER of 0.001 with $N = 32$ and 96 both, we get a transmit power gain of approximately 5.5 dB by choosing $J = 2$ as compared to $J = 1$, however, only a 2.5 dB additional gain is obtained by selecting 3 RISs. It can be seen from Fig. 7 that the analytical ABER curves closely follows the simulated ABER curves for almost all values of transmit power considered in the figure.

Observation 4: *It can be observed from Fig. 7 that ABER values reduces for higher NJ, however if NJ is same for two system configurations, the system with higher N outperforms the other one. One can see from Fig. 7 that for $NJ = 96$, we can have two possible combinations, i.e., $(N, J) = (96, 1)$ and $(N, J) = (32, 3)$ and it is clear from the figure that former combination (with higher N) outperforms the later. It is in line with Observation 1 for ACP performance.*

We have also compared the ABER performance of the proposed system (with outdated and imperfect CSI based RIS selection) with an ideal scenario (with perfect CSI based RIS selection, i.e., $\varrho_u[t] = 1, \delta^2_{e,u}[t] = 0$) in Fig. 7. It can be seen from Fig. 7 that under all the parameter settings considered in the figure, an approximate power loss of 2 dB is noted due to the imperfect and outdated CSI availability at the UAV.

In Fig. 8, the variations of ABER of User-1 under different binary modulation formats (e.g., BFSK, BPSK, and DPSK, used by the UAV for downlink transmission) are shown for two different LoS conditions of UAV-RIS ($|\mu_m[t]| = 1.8, 4.6$) and RIS-User-1 ($|\nu_m| = 1.12, 3.9$) links, for all $m \in \mathbb{M}$. For this figure, we have assumed that the UAV selects 3 RISs out of total 5 RISs available in the network. Firstly, it is clear from Fig. 8 that the derived analytical expression of ABER (with NCCS approximation) works well for different modulation formats under both the LoS conditions considered in the figure with $M = 5$ and $N = 96$. Moreover, the BPSK scheme outperforms the DPSK and BFSK schemes for all values of $|\mu_m[t]|$, $|\nu_m|$, and $\tilde{P}_U$ considered in the figure. It is also evident from Fig. 8 that the ABER of User-1 reduces significantly for strong LoS conditions of UAV-RIS and RIS-User links under all types of RF binary modulation formats. Fig. 8 also shows the impact of channel estimation error ($\delta^2_{e,u}[t]$) at the UAV on

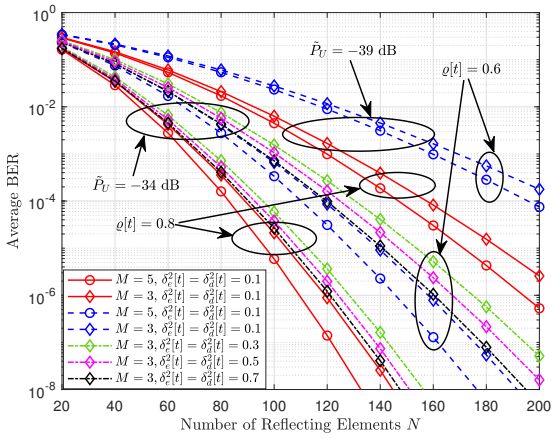

Fig. 9: Variations of ABER of User-1 w.r.t. number of reflecting elements at each RIS with $J = 2$ and different values of M, $\tilde{P}_U$, $\varrho[t], \delta_e^2[t]$, and $\delta_d^2[t]$. For the case of $M = 3$, the RISs are assumed to be located at $\boldsymbol{\chi}_{R_1}$, $\boldsymbol{\chi}_{R_2}$, and $\boldsymbol{\chi}_{R_3}$.

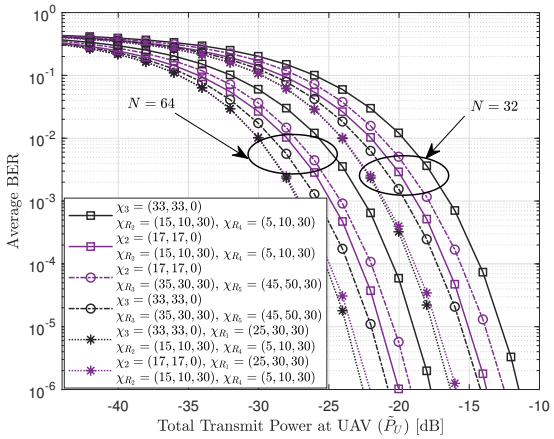

Fig. 10: ABER versus UAV transmit power performance for different user locations and RIS locations with $N = 32, 64$, $J = 1$, and $M = 2, 3$.

the ABER performance under a fixed outdated error condition at UAV (i.e., $\varrho_u[t] = 0.8$ and $\delta_{d,u}^2[t] = 0.1$).

Observation 5: *It is noteworthy from Fig. 8 that for high values of $\delta_{e,u}^2[t]$, the ABER performance under weak LoS conditions is affected severely under all binary modulation schemes considered. For example, considering BPSK scheme at $\delta_{e,u}^2[t] = 0.7$ with $|\mu_m[t]| = 1.8, |\nu_m| = 1.12$, an ABER of 10^{-4} is achieved at $\tilde{P}_U = -36$ dB as compared to -38.2 dB for $\delta_{e,u}^2[t] = 0.1$. Whereas at $|\mu_m[t]| = 4.6, |\nu_m| = 3.9$, the similar ABER is obtained at $\tilde{P}_U = -46$ dB and $\tilde{P}_U = -45.5$ dB for $\delta_{e,u}^2[t] = 0.7$ and $\delta_{e,u}^2[t] = 0.1$, respectively.*

Fig. 9 shows the variations in ABER performance of User-1 for varying number of reflecting elements at each RIS under two different values of M and $\tilde{P}_U$. For this, we have assumed equal parameters for imperfect and outdated CSIs at both UAV and the user, i.e., we have assumed (i) $\delta_{0,e,k}^2[t] = \delta_{1,e,k}^2[t] = \delta_{e,u}^2[t] = \delta_e^2[t]$, (ii) $\delta_{0,d,k}^2[t] = \delta_{1,d,k}^2[t] = \delta_{d,u}^2[t] = \delta_d^2[t]$, and (iii) $\varrho_{0,k}[t] = \varrho_{m_j,k}[t] = \varrho_u[t] = \varrho[t]$, for all $t \in \mathbb{T}$. For all the curves in Fig. 9, we have assumed that 2 out of $M(> 2)$ RISs are selected in each time slot. It can be observed from Fig. 9 that availability of more RISs in the network may not always provide a significant performance gain, if the size of each RIS is very small. However, beyond certain value of N, the performance gain due to increase in M are noticeable for all values of $\varrho[t], \delta_e^2[t]$, and $\delta_d^2[t]$ considered in the figure.

Observation 6: *Increasing M from 3 to 5 with $\tilde{P}_U = -39$ dB and $\varrho[t] = 0.8$ provides an ABER reduction from 0.0063 to 0.0045 at $N = 100$, whereas for $N = 200$, the ABER values reduces from 2.56×10^{-6} to 5.3×10^{-7}. It should also be noted from Fig. 9 that higher transmit power at UAV provides higher performance gain for increasing M. For example, at $\varrho[t] = 0.6$, the ABER values at $\tilde{P}_U = -39$ dB and $N = 160$ reduces from 0.0016 to 0.001 for increasing M from 3 to 5, whereas for same $\varrho[t]$, N with $\tilde{P}_U = -34$ dB, the ABER values reduces from 7.86×10^{-7} to 1.3×10^{-7}.*

We have also shown the impact varying normalized error variances, i.e., $\delta_e^2[t], \delta_d^2[t]$ on the ABER performance of the User-1 for $M = 3$, $\tilde{P}_U = -34$ dB, and $\varrho[t] = 0.6, 0.8$ in Fig. 9. It is evident from Fig. 9 that increasing the error variances (due to outdated and imperfect CSIs), the deterioration in the ABER performance is higher for low values of $\varrho[t]$.

In Fig. 10, we have shown the impact of RIS locations on the ABER performance of different users for varying N with BPSK modulation scheme. For all the curves in Fig. 10, we have assumed that the UAV selects a single RIS out of the multiple available RISs in each time slot. In Fig. 10, we have considered User-2 and User-3 located at $(17, 17, 0)$ and $(33, 33, 0)$, respectively. At first, we have considered 3 RISs with 3D locations $\boldsymbol{\chi}_{R_1}$, $\boldsymbol{\chi}_{R_2}$, and $\boldsymbol{\chi}_{R_4}$ and have plotted the ABER performance of User-2 and User-3 for $N = 32, 64$. It can be seen from Fig. 10 that for the above mentioned RIS locations, the ABER performance of User-2 and User-3 is nearly same. Next, we have plotted the performance for 2 RISs with 3D locations $\boldsymbol{\chi}_{R_2}$, $\boldsymbol{\chi}_{R_4}$ and have observed that User-2 significantly outperforms User-3 because both the RISs are closer User-2 as compared to User-3. If the RIS locations of 2 RISs are changed to $\boldsymbol{\chi}_{R_3}$ and $\boldsymbol{\chi}_{R_5}$, it can be noticed that User-3 outperforms User-2 as the new RIS locations are nearer to User-3. The behavior is same for both the values of N considered in the figure. Thus, it can be deduced from Fig. 10 that the performance of a ground user is not only affected by the number of RISs available in the network, number of RISs selected by the UAV, number of reflecting elements at each RIS, but also by the location of the RISs.

VII. Conclusions

We considered a multiple RIS-assisted downlink wireless communication system with a flying UAV transmitter and analyzed the system performance with a selection strategy of a set of RISs at the UAV. In particular, we considered that the UAV can select a set of RISs based on the composite UAV-RIS-User channel gains with the possibility of imperfect and outdated CSI of the composite links. The communication between the UAV and the user is accomplished through the selected RISs along with a direct link. We have derived series-based expression for the probability of selection of RISs under imperfect and outdated CSI based schemes. Moreover, we obtained the statistical distribution for instantaneously received SNR at the user and derived the expressions for

approximate ACP and ABER for overall UAV flight time at a given user. The asymptotic performances of the considered system have also been examined for small as well as large values of transmit power at UAV. The derived approximate analytical results were compared with exact simulated values and useful insights were obtained. It has been deduced from the results that it is always better to select fewer large-sized RISs as compared to selecting more small-sized RISs, for a fixed number of total reflecting elements in the network. In the end, we have investigated the impact of the severity of channel fading of UAV-RIS and RIS-User links along with the imperfect and outdated CSI on the network's performance.

REFERENCES

[1] S. Hayat, E. Yanmaz, and R. Muzaffar, "Survey on unmanned aerial vehicle networks for civil applications: A communications viewpoint," *IEEE Commun. Surveys Tuts.*, vol. 18, no. 4, pp. 2624–2661, Fourthquarter 2016.

[2] L. Gupta, R. Jain, and G. Vaszkun, "Survey of important issues in UAV communication networks," *IEEE Commun. Surveys Tuts.*, vol. 18, no. 2, pp. 1123–1152, Secondquarter 2016.

[3] D. C. Nguyen, M. Ding, P. N. Pathirana, A. Seneviratne, J. Li, and H. V. Poor, "Federated learning for internet of things: A comprehensive survey," *IEEE Commun. Surveys Tuts.*, vol. 23, no. 3, pp. 1622–1658, Thirdquarter 2021.

[4] L. Zhang, A. Celik, S. Dang, and B. Shihada, "Energy-efficient trajectory optimization for UAV-assisted IoT networks," *IEEE Trans. Mobile Comput.*, pp. 1–1, 2021.

[5] E. Boshkovska, D. W. K. Ng, N. Zlatanov, and R. Schober, "Practical non-linear energy harvesting model and resource allocation for SWIPT systems," *IEEE Commun. Lett.*, vol. 19, no. 12, pp. 2082–2085, 2015.

[6] W. Feng, J. Wang, Y. Chen, X. Wang, N. Ge, and J. Lu, "UAV-aided MIMO communications for 5G internet of things," *IEEE Internet Things J.*, vol. 6, no. 2, pp. 1731–1740, 2019.

[7] P. Raut, K. Singh, C.-P. Li, M.-S. Alouini, and W.-J. Huang, "Nonlinear EH-based UAV-assisted FD IoT networks: Infinite and finite blocklength analysis," *IEEE Internet Things J.*, vol. 8, no. 24, pp. 17 655–17 668, 2021.

[8] R. Han, J. Wang, L. Bai, J. Liu, and J. Choi, "Age of information and performance analysis for UAV-aided IoT systems," *IEEE Internet Things J.*, vol. 8, no. 19, pp. 14 447–14 457, 2021.

[9] X. Liu, Z. Liu, and M. Zhou, "Fair energy-efficient resource optimization for green multi-NOMA-UAV assisted internet of things," *IEEE Trans. Green Commun. Netw.g*, pp. 1–1, 2021.

[10] N. Nouri, J. Abouei, A. R. Sepasian, M. Jaseemuddin, A. Anpalagan, and K. N. Plataniotis, "Three-dimensional multi-UAV placement and resource allocation for energy-efficient IoT communication," *IEEE Internet Things J.*, vol. 9, no. 3, pp. 2134–2152, 2022.

[11] C. Zhan and R. Huang, "Energy efficient adaptive video streaming with rotary-wing UAV," *IEEE Trans. Veh. Technol.*, vol. 69, no. 7, pp. 8040–8044, 2020.

[12] C. Qiu, Z. Wei, Z. Feng, and P. Zhang, "Backhaul-aware trajectory optimization of fixed-wing UAV-mounted base station for continuous available wireless service," *IEEE Access*, vol. 8, pp. 60 940–60 950, 2020.

[13] Q. Wu and R. Zhang, "Intelligent reflecting surface enhanced wireless network via joint active and passive beamforming," *IEEE Trans. Wireless Commun.*, vol. 18, no. 11, pp. 5394–5409, 2019.

[14] A. Bansal, K. Singh, B. Clerckx, C.-P. Li, and M.-S. Alouini, "Rate-splitting multiple access for intelligent reflecting surface aided multi-user communications," *IEEE Trans. Veh. Technol.*, vol. 70, no. 9, pp. 9217–9229, 2021.

[15] Y. Yang, B. Zheng, S. Zhang, and R. Zhang, "Intelligent reflecting surface meets OFDM: Protocol design and rate maximization," pp. 4522–4535, 2020.

[16] C. Huang, A. Zappone, G. C. Alexandropoulos, M. Debbah, and C. Yuen, "Reconfigurable intelligent surfaces for energy efficiency in wireless communication," *IEEE Trans. Wireless Commun.*, vol. 18, no. 8, pp. 4157–4170, 2019.

[17] G. Zhou, C. Pan, H. Ren, K. Wang, and A. Nallanathan, "Intelligent reflecting surface aided multigroup multicast MISO communication systems," *IEEE Trans. Signal Process.*, vol. 68, pp. 3236–3251, 2020.

[18] E. Basar, M. Di Renzo, J. De Rosny, M. Debbah, M.-S. Alouini, and R. Zhang, "Wireless communications through reconfigurable intelligent surfaces," *IEEE Access*, vol. 7, pp. 116 753–116 773, 2019.

[19] M. A. Al-Jarrah, E. Alsusa, A. Al-Dweik, and M.-S. Alouini, "Performance analysis of wireless mesh backhauling using intelligent reflecting surfaces," *IEEE Trans. Wireless Commun.*, vol. 20, no. 6, pp. 3597–3610, 2021.

[20] M. Al-Jarrah, E. Alsusa, A. Al-Dweik, and D. K. C. So, "Capacity analysis of IRS-based UAV communications with imperfect phase compensation," *IEEE Wireless Commun. Lett.*, vol. 10, no. 7, pp. 1479–1483, 2021.

[21] A. Al-Dweik, M. A. Al-Jarrah, E. Alsusa, M.-S. Alouini, and Y. Iraqi, "IRS-assisted UAV communications with imperfect phase compensation," *IEEE Wireless Commun. Lett.*, 2020.

[22] T. Shafique, H. Tabassum, and E. Hossain, "Optimization of wireless relaying with flexible UAV-borne reflecting surfaces," 2020. [Online]. Available: https://arxiv.org/abs/2006.10969

[23] D. Xu, X. Yu, Y. Sun, D. W. K. Ng, and R. Schober, "Resource allocation for IRS-assisted full-duplex cognitive radio systems," *IEEE Trans. Commun.*, vol. 68, no. 12, pp. 7376–7394, 2020.

[24] C. You, Z. Kang, Y. Zeng, and R. Zhang, "Enabling smart reflection in integrated air-ground wireless network: IRS meets UAV," *arXiv*, 2021. [Online]. Available: https://arxiv.org/abs/2103.07151

[25] W. Wang, H. Tian, W. Ni, and M. Hua, "Intelligent reflecting surface aided secure UAV communications," *arXiv*, 2020. [Online]. Available: https://arxiv.org/abs/2011.04339

[26] Z. Wei, Y. Cai, Z. Sun, D. W. Kwan Ng, and J. Yuan, "Sum-rate maximization for IRS-assisted UAV OFDMA communication systems," in *Proc. IEEE Global Communications Conference*, Dec. 2020, pp. 1–7.

[27] L. Ge, P. Dong, H. Zhang, J.-B. Wang, and X. You, "Joint beamforming and trajectory optimization for intelligent reflecting surfaces-assisted UAV communications," *IEEE Access*, vol. 8, pp. 78 702–78 712, Apr. 2020.

[28] S. Fang, G. Chen, and Y. Li, "Joint optimization for secure intelligent reflecting surface assisted UAV networks," *IEEE Wireless Commun. Lett.*, vol. 10, no. 2, pp. 276–280, Feb. 2021.

[29] A. Mahmoud, S. Muhaidat, P. Sofotasios, I. Abualhaol, O. A. Dobre, and H. Yanikomeroglu, "Intelligent reflecting surfaces assisted UAV communications for IoT networks: Performance analysis," *IEEE Trans. Green Commun. Netw.*, pp. 1–1, 2021.

[30] Z. Wei, Y. Cai, Z. Sun, D. W. K. Ng, J. Yuan, M. Zhou, and L. Sun, "Sum-rate maximization for IRS-assisted UAV OFDMA communication systems," *IEEE Trans. Wireless Commun.*, vol. 20, no. 4, pp. 2530–2550, 2021.

[31] H. Gao, K. Cui, C. Huang, and C. Yuen, "Robust beamforming for RIS-assisted wireless communications with discrete phase shifts," *IEEE Wireless Commun. Lett.*, vol. 10, no. 12, pp. 2619–2623, 2021.

[32] Z. Li, W. Chen, Q. Wu, H. Cao, K. Wang, and J. Li, "Robust beamforming design and time allocation for IRS-assisted wireless powered communication networks," *IEEE Trans. Commun.*, vol. 70, no. 4, pp. 2838–2852, 2022.

[33] Y. Wang, X. Chen, Y. Cai, and L. Hanzo, "RIS-aided hybrid massive MIMO systems relying on adaptive-resolution ADCs: Robust beamforming design and resource allocation," *IEEE Trans. Veh. Technol.*, vol. 71, no. 3, pp. 3281–3286, 2022.

[34] X. Guo, Y. Chen, and Y. Wang, "Learning-based robust and secure transmission for reconfigurable intelligent surface aided millimeter wave UAV communications," *IEEE Wireless Commun. Lett.*, vol. 10, no. 8, pp. 1795–1799, Aug. 2021.

[35] S. Li, B. Duo, M. D. Renzo, M. Tao, and X. Yuan, "Robust secure UAV communications with the aid of reconfigurable intelligent surfaces," *IEEE Trans. Wireless Commun.*, vol. 20, no. 10, pp. 6402–6417, 2021.

[36] J. Zhao, L. Yu, K. Cai, Y. Zhu, and Z. Han, "RIS-aided ground-aerial NOMA communications: A distributionally robust DRL approach," *IEEE J. Sel. Areas Commun.*, vol. 40, no. 4, pp. 1287–1301, 2022.

[37] K. K. Nguyen, A. Masaracchia, V. Sharma, H. V. Poor, and T. Q. Duong, "RIS-assisted UAV communications for IoT with wireless power transfer using deep reinforcement learning," *IEEE J. Sel. Top. Signal Process.*, vol. 16, no. 5, pp. 1086–1096, 2022.

[38] L. Wei, C. Huang, G. C. Alexandropoulos, C. Yuen, Z. Zhang, and M. Debbah, "Channel estimation for RIS-empowered multi-user MISO wireless communications," *IEEE Trans. Commun*, vol. 69, no. 6, pp. 4144–4157, 2021.

[39] G. Zhou, C. Pan, H. Ren, K. Wang, and A. Nallanathan, "A framework of robust transmission design for IRS-aided MISO communications with imperfect cascaded channels," *IEEE Trans. Signal Process.*, vol. 68, pp. 5092–5106, 2020.

[40] X. Wang, Z. Fei, J. Guo, Z. Zheng, and B. Li, "RIS-assisted spectrum sharing between MIMO radar and MU-MISO communication systems," *IEEE Wireless Commun. Lett.*, vol. 10, no. 3, pp. 594–598, 2021.
[41] Y. Zeng, J. Xu, and R. Zhang, "Energy minimization for wireless communication with rotary-wing UAV," *IEEE Trans. Wireless Commun.*, vol. 18, no. 4, pp. 2329–2345, 2019.
[42] Z. Chu, Z. Zhu, X. Li, F. Zhou, L. Zhen, and N. Al-Dhahir, "Resource allocation for IRS-assisted wireless-powered FDMA IoT networks," *IEEE Internet Things J.*, vol. 9, no. 11, pp. 8774–8785, Jun. 2022.
[43] A. Papoulis, *Probability, Random Variables and Stochastic Processes*. McGraw-Hill, 2002.
[44] I. S. Gradshteyn and I. M. Rhyzhik, *Table of integrals, series and products*. A. Jeffrey and D. Zwillinger, Academic Press, 2007.
[45] W. R. Inc., "The mathematical functions site," champaign, IL, 2022. [Online]. Available: https://functions.wolfram.com/
[46] I. S. Ansari, S. Al-Ahmadi, F. Yilmaz, M.-S. Alouini, and H. Yanikomeroglu, "A new formula for the ber of binary modulations with dual-branch selection over generalized-k composite fading channels," *IEEE Trans. Commun.*, vol. 59, no. 10, pp. 2654–2658, 2011.

Ankur Bansal (**Member, IEEE**) completed his Masters in Signal Processing from Division of ECE, NSIT, Delhi, in 2009 and received his Ph.D. Degree from Department of Electrical Engineering, Indian Institute of Technology (IIT) Delhi, India in 2013. He served as Assistant Professor in Division of ECE, NSIT from September 2013 to December 2019. Currently he is working as an Assistant Professor in Department of Electrical Engineering, IIT Jammu since December 2019. His main research interests include multiple-input multiple-output (MIMO) communications, multi-user communications with energy harvesting in UAV-assisted networks, free space optical communications, and intelligent reflecting surface (IRS) assisted communication systems. Moreover, he has published several research papers in reputed international journals like IEEE TVT, IEEE TWC, IET Communications, and IEEE/OSA JOCN etc. He has also presented papers in various conferences like IEEE VTC, IEEE ICC, IEEE SPCOM, and NCC etc. Dr. Bansal has been an active member of IEEE since 2012 and has also served as a reviewer of various IEEE journals and conferences.

Neelima Agrawal (**Member, IEEE**) is a Post-Doctoral fellow with the Institute of Communications Engineering, National Sun Yat-sen University, Kaohsiung 80424, Taiwan, R.O.C. She received B.Tech. degree in Electrical and Electronics Engineering from the Uttar Pradesh Technical University, Lucknow in 2012 and M.Tech. degree in Power Electronics and Drives in 2015 from the Madan Mohan Malaviya University of Technology, Gorakhpur. She obtained a Ph. D degree in Electronics and Communication Engineering in 2019 from Visvesvaraya National Institute of Technology, Nagpur, India. Her current research interests include wireless communications, IRS assisted UAV based communication and vehicular communication.

Keshav Singh (**Member, IEEE**) received the M.Sc. degree in Information and Telecommunications Technologies from Athens Information Technology, Greece, in 2009, and the Ph.D. degree in Communication Engineering from National Central University, Taiwan, in 2015. He currently works at the Institute of Communications Engineering, National Sun Yat-sen University (NSYSU), Taiwan as an Assistant Professor. Prior to this, he held the position of Research Associate from 2016 to 2019 at the Institute of Digital Communications, University of Edinburgh, U.K. From 2019 to 2020, he was associated with the University College Dublin, Ireland as a Research Fellow. He leads research in the areas of green communications, resource allocation, transceiver design for full-duplex radio, ultra-reliable low-latency communication, non-orthogonal multiple access, wireless edge caching, machine learning for wireless communications, and large intelligent surface assisted communications.

Chih-Peng Li (**Fellow, IEEE**) received the B.S. degree in Physics from National Tsing Hua University, Hsin Chu, Taiwan, and the Ph.D. degree in Electrical Engineering from Cornell University, NY, USA. Dr. Li was a Member of Technical Staff with Lucent Technologies. Since 2002, he has been with National Sun Yat-sen University (NSYSU), Kaohsiung, Taiwan, where he is currently a Distinguished Professor. Dr. Li has served various positions with NSYSU, including the Chairman of Electrical Engineering Department, the VP of General Affairs, the Dean of Engineering College, and the VP of Academic Affairs. His research interests include wireless communications, baseband signal processing, and data networks. He is now the Director General with the Engineering and Technologies Department, National Science and Technology Council, Taiwan.

Dr. Li is currently the Chapter Chair of IEEE Broadcasting Technology Society Tainan Section. Dr. Li has also served as the Chapter Chair of IEEE Communication Society Tainan Section, the President of Taiwan Institute of Electrical and Electronics Engineering, the Editor of IEEE Transactions on Wireless Communications, the Associate Editor of IEEE Transactions on Broadcasting, and the Member of Board of Governors with IEEE Tainan Section. Dr. Li has received various awards, including the Outstanding Research Award of Ministry of Science and Technology. Dr. Li is a Fellow of the IEEE.

Shahid Mumtaz (**Senior Member, IEEE**) is a Professor at the University of Technology Akademicka, Gliwice, Poland and the Nottingham Trent University, Nottingham, UK. He is an IET Fellow, founder, and EiC of IET "Journal of Quantum Communication," Vice-Chair: Europe/Africa Region- IEEE ComSoc: Green Communications & Computing Society. He authorizes four technical books, 12 book chapters, and 300+ technical papers (200+ IEEE Journals/transactions, 100+ conferences, 2 IEEE best paper awards) in mobile communications. Most of his publication is in the field of Wireless Communication. He is a Scientific Expert and Evaluator for various research funding agencies. In 2012, he was awarded an "Alain Bensoussan fellowship." China awarded him the young scientist fellowship in 2017.